Variability of local stress states resulting from the application of Monte Carlo and finite difference methods to the stability study of a selected slope

Pasculli Antonio*, Calista Monia, Sciarra Nicola

Department of Engineering and Geology (INGEO), University of Chieti-Pescara, Chieti (Italy)

* corresponding author:

Department of Engineering and Geology (INGEO), University of Chieti-Pescara (Italy)

Via dei Vestini 30, 66013 Chieti University G. d'Annunzio Chieti-Pescara (Italy)

Office phone number: 39 0871 355 6159; fax: 39 0871 355 5364

e-mail: antonio.pasculli@unich.it

Abstract

In slope stability analysis it is decisive to represent, in the most realistic way, the heterogeneity of the soil characteristics. The Monte Carlo technique is one of the suitable mathematical tools that could be useful for this purpose. The result of this kind of approach is a set of multiple possible realizations of the same system, characterized by different spatial distribution of the numerical values of the geotechnical parameters. The numerical stress states outcomes, obtained through a stability analysis, would depend on the models employed to define the spatial parameters distribution and, further, on the utilized geomechanical models. Accordingly, first of all, we selected a suitable mathematical model, based on the Monte Carlo technique. Then, we integrated it into a commonly used FDM (Finite Difference Method) commercial code (FLAC2D). Finally, we studied the stability of an actual slope, considered as a test case (Lettomanoppello, Chieti, Italy), whose geological and geomechanical characteristics make it suitable for the application of the selected code. In this step, in order to simplify the analyses, we considered only dry conditions. Therefore, we discussed how the stochastic distributions of the local stress states, resulting from hundreds of repeated runs, were correlated to the mechanical parameters distributions obtained by the Monte Carlo application and assigned to each points as inputs. The results of the test application suggest that our approach can be used to identify sectors of the slopes more sensitive to the variability of the input values of the main geotechnical parameters, which would require a more accurate modelling and monitoring.

Keywords: numerical modeling; geological modeling; random parameters distribution; Monte Carlo method; statistics.

1. Introduction

A suitable and effective mathematical tool, capable to include the complexity of soil structures, caused also by weathering (Esposito et al. 2013; Pasculli et al., 2017) may be provided by statistical approaches. Some authors, including Vanmarcke (1977), Fenton and Vanmarke (1990), Rabczuk et al. (2007), Andrade et al. (2008), Bossi et al. (2016), Vu-Bac et al. (2016), highlighted the importance of considering the possible numerical values of the geotechnical parameters as random variables, belonging to an assumed Probability Distribution Function (PDF), for example a Gaussian Function, particularly in the case of the study of the stability of granular media. Of course, the obtained results were based on algorithms that can calculate random numerical values. Current computing techniques are not able to generate truly random numbers. Many strategies were proposed, based, for instance, on the internal clock of the computer (Banks et al., 2005). However, all the generated sets of numerical values have a cyclicity. Accordingly, after a certain number of generations, even if very long (10^{36} as well), the obtained sequences repeat themselves. For this reason the values are called 'pseudo-random numbers'. The PDF can be acquired as the outcome of multiple runs, all with the same inputs, but with different parameter values, computed automatically by a selected mathematical algorithm based on pseudo-random generation, integrated as intrinsic routine into most codes. This kind of approach is called 'Monte Carlo', already applied in the field of slope stability analyses (among many others: Sundell et al., 2016). In the context of the study of slope stability, many geomechanical and mathematical-numerical approaches have been proposed in the international literature. Among these, Rabczuk and Areias (2006) and Rabczuk et al. (2007) proposed interesting approaches for modeling shear bands with cohesive geological materials, through the important mesh-free numerical technique, which avoids the cumbersome construction of meshes, like *Smoothed Particle Hydrodynamics* (SPH). This kind of approach was long used in many fields including those where it is necessary to simulate large deformations or transition from solid-like to fluid like of the materials or in the study of debris flow (among many others, Minatti and Pasculli 2010, 2011, Pasculli et al. 2013, 2014). However, despite these techniques are very valid, the most common commercial computer codes such as those belonging to the FLAC family, widely and commonly used in professional practice, are based on different approaches. Consequently, for the purpose of this paper, we have selected this type of computer code, in its 2D version. FLAC2D is based on Finite Difference Method (FDM) applied to continuum mechanics (among many others: Jiang et al. 2001; Sitharam et

al. 2007; Calista et al. 2015a, 2015b, 2016;). The continuum is discretized by a grid as suitable as possible for the system under study, faults and sliding surfaces included. A significant feature of the FLAC2D code is the option for assigning the numerical values of the geotechnical parameters or suitable constitutive equations to each grid cell, according to specific rules selected by the user, through the interactive language called FISH (based on the C compiler). At this stage of the research, for the sake of simplicity, the connectivity between the value of mechanical parameters assigned to a point and the values of near others points was not implemented, observing that the common experimental connectivity scale (less than 1 meter, Vanmarke, 1977; Ching and Wang, 2016) was lower than the selected dimension of the average distance among points (ranging from 10 to 20 meters) resulting from the selected discretization of the continuum. Some applications to actual slope systems, using both FLAC2D and FLAC3D, can already be found in Calista et al. (2015a and b), Pasculli and Sciarra (2006a), Pasculli et al., (2006b), Sciarra et al., (2006), where the first attempts to exploit Monte Carlo techniques not only for 2D, but also for 3D simulations, were pursued. However, the works available in the framework of the international literature, among which Vanmarke (1977), Fenton and Vanmarke (1990) and more recently Bossi et al. (2016), Ching and Wang, (2016), Sundell et al. (2016), have not sufficiently deepened yet the important issue of how common numerical approaches, exploited by the most used commercial computer, may influence and modify the spatial propagation of the uncertainties. Accordingly, for the sake of simplicity, we proposed an approach considering a surrogate deterministic dependence of all geotechnical variables on just one parameter: the Unit volume weight. The comparisons between the variability of the inputs and outputs data, resulting from the application of FLAC, were carried out, according to the scope of the paper, by the commonly utilized commercial code STATGRAPHICS Centurion XVI, 2010. Available options were reported in Table A.1, ‘Exploited statistical tools’, and in Table A.2, ‘Fitting curve’ (Cox and Hinkley, 1974, Casella and Berger, 2001). Then, after this type of analysis, for particular identified sectors of the system under study, an enhanced modelling, like multivariate approach, may be required as a successive step. Recently, Vu-Bac et al. (2016) and Hamdia et al. (2017) have proposed an interesting approach aimed at realizing a global sensitivity analysis of the variables that affect the selected system in order to quantify the significance of the input parameters and their joint effects on the output by varying all the parameters at the same time. In these two papers the polynomial chaos expansions (Ghanem and Spanos,1991) were applied. However, Ghanem and Spanos (1991) also exploited the Monte Carlo method in order to test the analytical chaos expansions. Thus, in our paper, we found reasonable to select a model based on the Monte Carlo method (Pasculli and Sciarra (2002, 2003) as an effective alternative to chaos function expansion. Moreover a Yielding Index (F_{YI}), similar to a local safety factor, on which the global factor may depend, calculated in each mesh of the

numerically discretized continuum, was introduced as an indicative parameter of the local stress state and of the possible local risk of rupture. Usually, the uncertainties related to the determination of important physical and geotechnical parameters can be introduced by assigning a PDF of these parameters to each node of the discretized spatial domain. Accordingly, the calculated values of parameters that depend on these quantities, such as for example the local stability factors, will be affected by some variability and uncertainties, described by the resulting PDFs, not necessarily similar to those provided for the input parameters. Therefore, the comparison between the input PDFs and the resulting calculated PDFs, can provide, as discussed below, the indications, at least for the system under study, on how the uncertainties introduced in the inputs propagated through the entire spatial domain. After a brief discussion of the mathematical model, details of the algorithm implementation are given. The interactive FISH code was used to make the FLAC2D more suitable for Monte Carlo multiple realizations of possible real structural configurations. For the purpose of this study, rainfall infiltration and filtration were not included. Accordingly, the selected slope was considered in dry conditions. Then, the results related to 650 Monte Carlo realizations of the spatial assignment of mechanical parameters values, belonging to a prior selected Gaussian numerical ensemble, based on real data and representative of an actual slope test case, are discussed. The choice of the number of realizations was conditioned by only the request to limit the calculation time. Finally, the statistical distributions of the cohesion coefficient related to the representative area of the slope, obtained through the Monte Carlo approach, were compared to the resulting distributions of the calculated F_{YI}, applying a commonly used commercial code (STATGRAPHICS).

2. Mathematical algorithms and code implementation description

For the sake of clarity, a brief sketch of the implemented mathematical model, already partially discussed in our previous works (Pasculli. and Sciarra 2003, 2006, for instance), is presented and more insights are given. Each mechanical parameter was assumed to be a random variable Ψ_{rand} , and accordingly, affected by some uncertainties. However, a sufficient number of samples, necessary to build a suitable statistics, is not always available, as in the case of the test selected for this work. On the other hand, an extensive bibliography is also dedicated to the description of the range of variability of the most important parameters characterizing the materials that constitute soils. Therefore, even for the purposes of the paper, we considered synthetic data based, however, on experimental values with the related variability drawn from the bibliography and reported in Table 1, regarding material resulting from the geophysical surveys carried out for the test case. In particular, the 'Unit volume weight' of the Clay material (γ_{rand}) was assumed to be a random variable Ψ_{rand}

affected, from Table 1, by the following uncertainties: $19.5\ (\mathrm{kN/m^3}) \leq \gamma_{rand} \leq 21.0\ (\mathrm{kN/m^3})$. Another important statistical parameter was the Standard deviation σ_Ψ that, following the adopted approach, had to be deduced from the data shown in the same Table 1. We estimated this parameter on the base of the well *Chebyshev inequality*, according to which about 93% of the numerical value of Ψ_{rand} lies in the range: $\Psi_{mean} - 4\sigma_\Psi \leq \Psi_{rand} \leq \Psi_{\mathrm{mean}} + 4\sigma_\Psi$, where $\Psi_{\mathrm{mean}} = (\Psi_{\mathrm{min}} + \Psi_{\mathrm{max}})/2$ was the estimated mean, (Clay: $\Psi_{\mathrm{mean}} = (19.5 + 21.0)/2 = 20.25\ \mathrm{kN/m^3}$), independently from the probability distribution function to which the random variable belongs. By consequence, we assumed that in general: $\Psi_{\mathrm{min}} = \Psi_{\mathrm{mean}} - 4\sigma_\Psi$, $\Psi_{\mathrm{max}} = \Psi_{\mathrm{mean}} + 4\sigma_\Psi$. Moreover the resulting standard deviation was estimated in the following way:

$$\sigma_\Psi = \frac{(\Psi_{\mathrm{max}} - \Psi_{\mathrm{min}})}{8} = 0.125 \cdot (\Psi_{\mathrm{max}} - \Psi_{\mathrm{min}}) \quad (1)$$

In particular, for the Clay: $\sigma_\Psi = \frac{(\Psi_{max} - \Psi_{\mathrm{min}})}{8} = 0.125 \cdot (\Psi_{max} - \Psi_{min}) = 0.125 \cdot (21.0 - 19.5) = 0.0625\ \mathrm{kN/m^3}$.

Following the above procedure, we were able to define the generic random variable, assumed suitable for simulating the numerical values of the mechanical parameters characterizing the soil under study:

$$\Psi_{rand} = \Psi_{mean} + (\sigma_\Psi \cdot g\_norm) \quad (2)$$

where:

$$g\_norm = \sqrt{[-2 \cdot ln(y\_ran1)]} \cdot cos(2\pi \cdot y\_ran2) \quad (3)$$

was the Standard Gaussian Distribution (SGD) provided by the algorithm proposed by Box and Muller (1958), while y_ran1 and y_ran2 were two non-correlated (pseudo) random variables uniformly distributed in the interval (0, 1) (provided directly by the FLAC's intrinsic function URAND). For the Clay: $\Psi_{rand}(\text{Unit volume weight}) \equiv \gamma_{rand} = [20.25 + (0.0625 \cdot g\_norm)]\ \mathrm{kN/m^3}$. Truncated probability distribution (Hesse et al., 2014) was not considered here, thus, by consequence, the SGD, and accordingly Eq. (3), may provide random values outside of the assumed range. Hence, in this case, the value was set equal to the mean. Furthermore, again for the sake of simplicity, we assumed that random spatial variations of each mechanical parameters were in direct accordance with the random spatial variation of the 'Unit volume weight' of the selected material (Deposits, Clay, Clay marl and Chalk alteration, Limestone) through a simple linear law:

$$\Psi_{rand}(x,y) = (\Psi_{max} - \Psi_{min}) \frac{[\gamma_{rand}(x,y) - \gamma_{min}]}{(\gamma_{max} - \gamma_{min})} + \Psi_{min} \quad (4)$$

where $\Psi_{rand}(x,y)$ and $\gamma_{rand}(x,y)$ were the stochastic numerical value of the selected parameter (friction, cohesion, elastic modulus) and the 'Unit volume weight' assigned to the point P(x,y), through the application of the proposed algorithm. Furthermore, an important underlying assumption was that the used statistical distribution was not spatially stationary. Now, through the above approach, the values of the parameter were estimated on only the basis of a pure application of statistics, without considering the alteration due to the specific conditions and interactions to which each sample would be affected in situ. Accordingly, a combination of a deterministic and random terms due, respectively, to the lithostatic pressure or other loads at macroscopic scale and to a local grains contact distribution at small scale had to be included.

Then the deviation of the in situ $\gamma_{rand\_insitu}(x,y)$ and the estimated value $\gamma_{rand\_lab}(x,y) = \gamma_{mean} + (\sigma_{\gamma\_lab} \cdot g\_norm1)$, to be measured in a 'virtual laboratory', resulting from the previous consideration in accordance with Eqs. (2) and (3), was assumed to be as much higher as the difference between the value that the selected parameter would have had if there had been only the deterministic term due to lithological deterministic load $\mu_\gamma(x,y)$ and the intrinsic random value of that parameter, $\gamma_{rand\_lab}(x,y)$, multiplied by a random factor ε:

$$\gamma_{rand\_insitu}(x,y) - \gamma_{rand\_lab}(x,y) = \left[\mu_\gamma(x,y) - \gamma_{rand\_lab}(x,y)\right] \cdot \varepsilon \quad (5)$$

The ε parameter was a random factor that 'weighed' the deviation between the deterministic trend and the random value of the parameter associated to the selected point P(x,y). The random factor was assumed to be a normal Gaussian term (with unitary mean and standard deviation) similar to Eq. (1) in which $(\Psi_{max} - \Psi_{min})$ was equal to one: $\varepsilon = 1. + 0.125 \cdot g\_norm2$. It should be noted that g_norm1 and g_norm2 were two different realizations of the SGD (Eq. 3), thus four non correlated (pseudo) random variables were requested. The deterministic term $\mu_\gamma(x,y)$ was assumed to be equal to the following relation:

$$\mu_\gamma(x,y) = (\gamma_{max} - \gamma_{min}) \frac{[h(x,y) - h_{min}(y)]}{[h_{max}(y) - \gamma_{min}(y)]} + \gamma_{min} \quad (6)$$

where: $h(x,y)$ was the depth of a generic point from the topographic level; $h_{min}(y)$ and $h_{max}(y)$ were, respectively, the minimum and the maximum depths at which a generic point embedded in a

specific sector, could be located (see lens in Fig. 1a). Fig. 1b shows the selected variation law of the parameters along depth. Finally, after simple manipulation, the following was the relation on which the implemented algorithms were based:

$$\gamma_{insitu}(x,y) = \mu_\gamma(x,y) + \left[\mu_\gamma(x,y) - \gamma_{mean}\right] \cdot 0.125 \cdot g\_norm2 - \sigma_\gamma \cdot 0.125 \cdot g\_norm1 \cdot g\_norm2 \quad (7)$$

In Appendix we reported a flow chart (Fig. A.1.) of the adopted algorithm and a figure (Fig. A.2.), freely adapted from Pasculli and Sciarra (2003).

Fig. 1. Sketch of a generic, synthetic slope: a) geometrical parameters exploited in the mathematical model; b) selected trend of the parameters along depth.

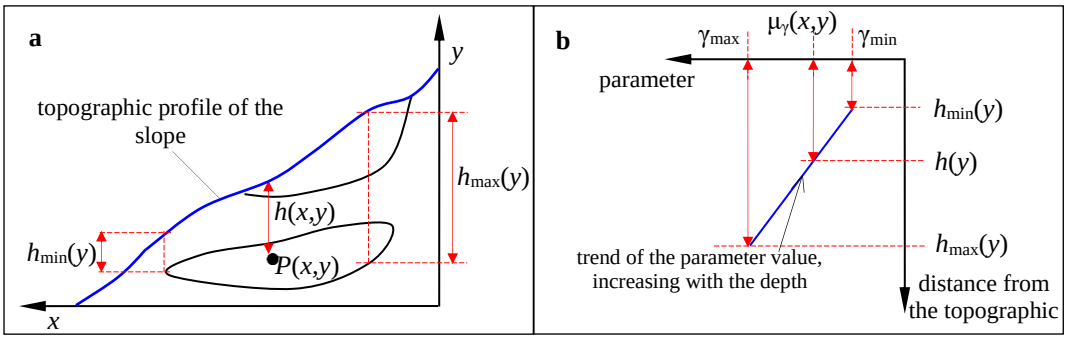

2.1. Monte Carlo implementation test

The proposed Monte Carlo approach was based on the elaboration of (pseudo) random numbers, uniformly distributed within the range [0, 1], obtained essentially through both intrinsic algorithms included by default into the operative system and the used numerical tools (commercial such as FLAC or implemented by compilers such as Fortran, or C++). In this paper, in order to provide a different random number distribution, such as Gaussian distribution, the algorithm proposed by Box and Muller (1958), previously detailed, was selected. However, for its correct utilization, the (pseudo) random variables y_ran1 and y_ran2 (Eq. 3), uniformly distributed in the interval [0, 1] and calculated in sequence, should not be correlated. Hence, in Fig. 2a, the generated couples of 10,000 pseudo random numbers, obtained by FLAC's intrinsic function URAND, are shown. In particular, along the abscissa and the ordinate axes, the i-th x random number corresponding to y_ran1 and the (i+1)-th x random number corresponding to y_ran2 , are respectively reported as black dot. The resulting dots distribution is clearly completely random (no trends at all). Thus, the absence of any correlation between x_i and successively generated x_{i+1} random number satisfies the requirement for the proper application of the Box Muller algorithm.

Fig. 2. a) Correlation test between x_i and successively generated x_{i+1} random numbers; b) Normality test; c) FLAC pseudo random numbers realization compared to Gaussian curve.

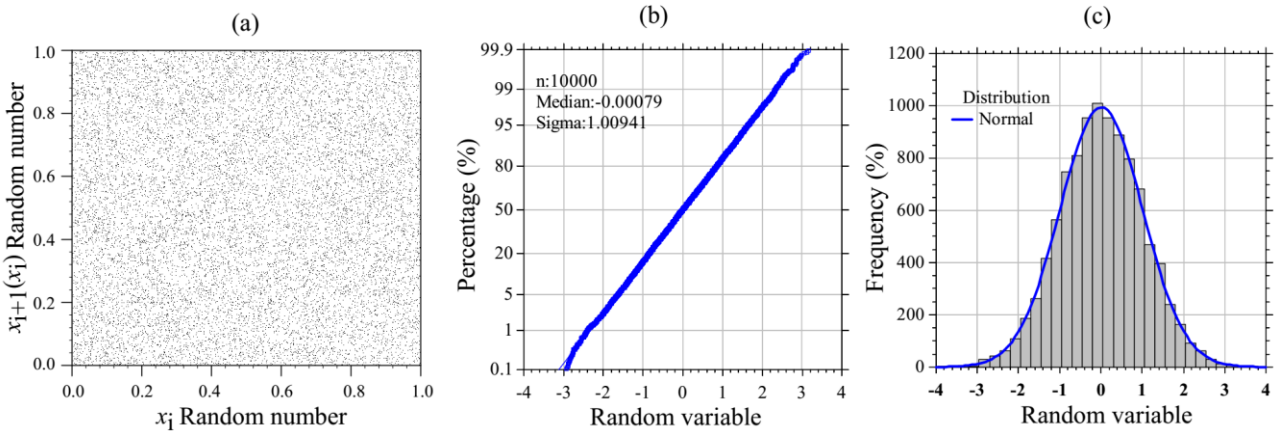

Despite a correct application of both the Box-Muller's algorithm and the FLAC's intrinsic routine URAND, the realization of the distribution of random numbers, however, may suffer from an asymmetry around the mean. As shown in Fig. 2b and c, the random number distribution function, obtained according to the above detailed approaches, on which the Monte Carlo strategy adopted in this paper is based, is affected by a slight negative skewness (James, 2006).

In short, the first step was to create a normal distribution of 10,000 random numbers (Fig. 2c). Accordingly, for each exploited mechanical parameter, an ensemble containing 10,000 possible random numerical values was generated through the expression (2), once for all the simulations. Then, at the beginning of each of the 650 realizations, the required numerical values input given by the expression (7), in particular the cohesion coefficients (function of the Unit volume weight, eq. 4) that should be assigned to each meshes, were randomly extracted from the associated ensemble by an automatic procedure. Thus, for each node, a different resulting statistical distribution of 650 F_{YI} numerical values was acquired. The cohesion coefficients were selected for further analyses and comparison.

2.2. FISH code implementation

In order to implement the algorithms briefly discussed above, we developed a FISH code, aimed at equipping the FLAC2D with the capability to apply Monte Carlo multiple realizations of possible actual structural configurations. In particular, Figs. A.3a and A.3b (in Appendix), show the FISH instructions, with some comments there reported, which were implemented in order to define, respectively, the distances from the topographic level of a selected point, as detailed in Fig. 1, and

the random value of the density assigned to it, following the algorithms characterized by Eqs. (2), (3), (4) and (5).

2.2.1. FISH implementation test

The algorithm, implemented into the FLAC2D, was first tested on a simple rectangular brick, using a 1 m wide and 5 m high grid, discretized with 0.1 m side square mesh. The aim of the proposed model is to attribute to each point geo-mechanical characteristics, affected by variability and, as a working hypothesis, by a linear trend with depth. Furthermore, each realization must be randomly different from the others. Accordingly, the Fig. 3b shows four different realizations with different random numerical values of the selected parameter (in this case the Unit volume weight), with a superimposed linear trend along the depth (Fig. 3a). The coloured contour plots of the four random realizations of the density and their graphs with the depth along a given vertical are reported. To this respect we can say that the results are 'reasonable' because they were the results we pursued to obtain.

Fig. 3. a) unit volume weight graphs in depth along the verticals A-A', B-B' and C-C';b) contour plots of the unit volume weight for 4 realization.

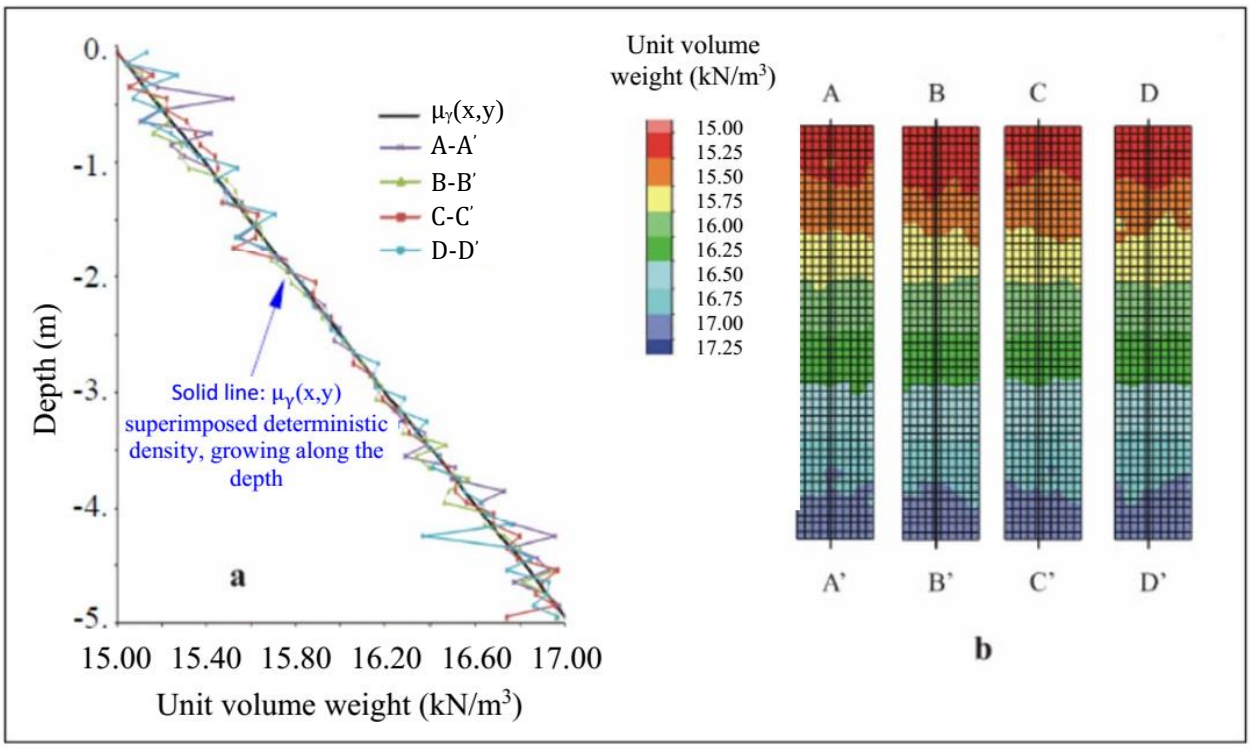

2.3. Yielding Index

The selected code is based on the Finite Difference Method (FDM). Accordingly, the continuum is divided in many meshes. In each mesh, the Mohr-Coulomb rupture criterion for all type of materials was selected. The 2D stress state within each mesh can be expressed in terms of principal stress σ_1 and σ_3 . In the Mohr-Coulomb diagram, the associated stress state is identified by a circle (circle 'a' in Fig. 4 freely adapted from Itasca Manual), characterized by a radius r_a. The element will reach the rupture conditions when the circle will be tangent to the envelope of rupture (circle 'b' in Fig. 4) defined, according to the Mohr-Coulomb criterion, through the well-known relation: $\tau = c' + \sigma' tan\varphi'$, where τ , c' , σ' and φ' are, respectively, the failure shear stress, the applied effective normal stress, the effective angle of internal friction. In this paper we assumed that the values of the mechanical parameters are referred to dry conditions. The ratio between the radii of the two circles may be defined as 'Yielding Index', $F_{YI} = r_a/r_b$, somehow representing a local factor of safety. The Yielding Index F_{YI} was selected as the key parameter for analyzing and collecting the results coming from 650 different realizations.

Fig. 4. Mohr-Coulomb diagram (freely adapted from FLAC manual).

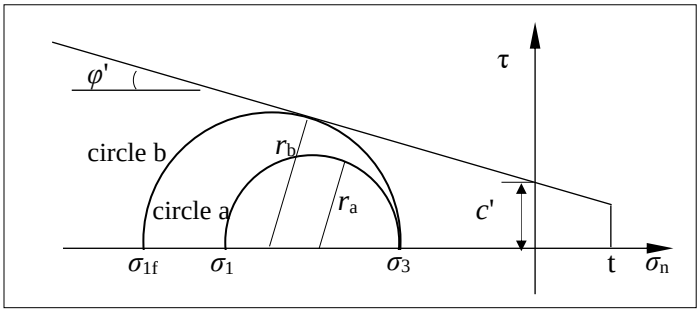

3. Test case

The above discussed methodology was applied to an actual slope section. The study area, selected as test case, is situated close to the town of Lettomanoppello (Pescara, Italy). It is located in the central-eastern margin of the Apennines, along the north-western foothills of the relief of the Maiella (Fig. 5).

Fig. 5. Geographic map of the investigated area

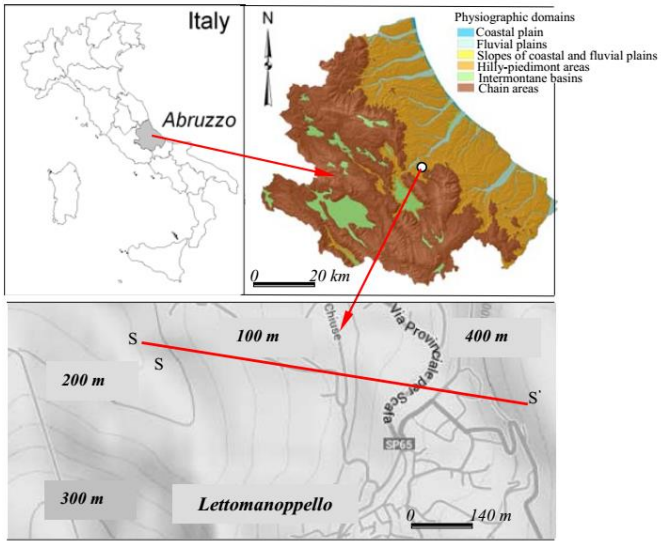

The slope, on which the village of Lettomanoppello is located, is historically known for its susceptibility to landslides. In fact, the literature sources indicate continuing movements since 1908. The area includes Quaternary continental deposits (detritus deposits, limestone debris hetero-metric, landslide body) and Mio-Pleistocene marine deposits (clay; clay, marl and chalk alternation; limestone). The proposed approach was applied to a particularly significant section (section S-S' in Fig. 5). In Fig. 6, the related outline of the section and the numerical FLAC grid, are reported. As shown in Fig. 6a, the geological section is particularly complex because it features numerous sub vertical faults and, in particular, a surface of discontinuity between Quaternary continental deposits and Mio-Pleistocene marine deposits.

Fig. 6. a) Geological section (section S-S', Fig. 5); b) grid used for modelling; c) density variation with depth; d) friction variation with the depth; e) bulk modulus and shear modulus variation with depth.

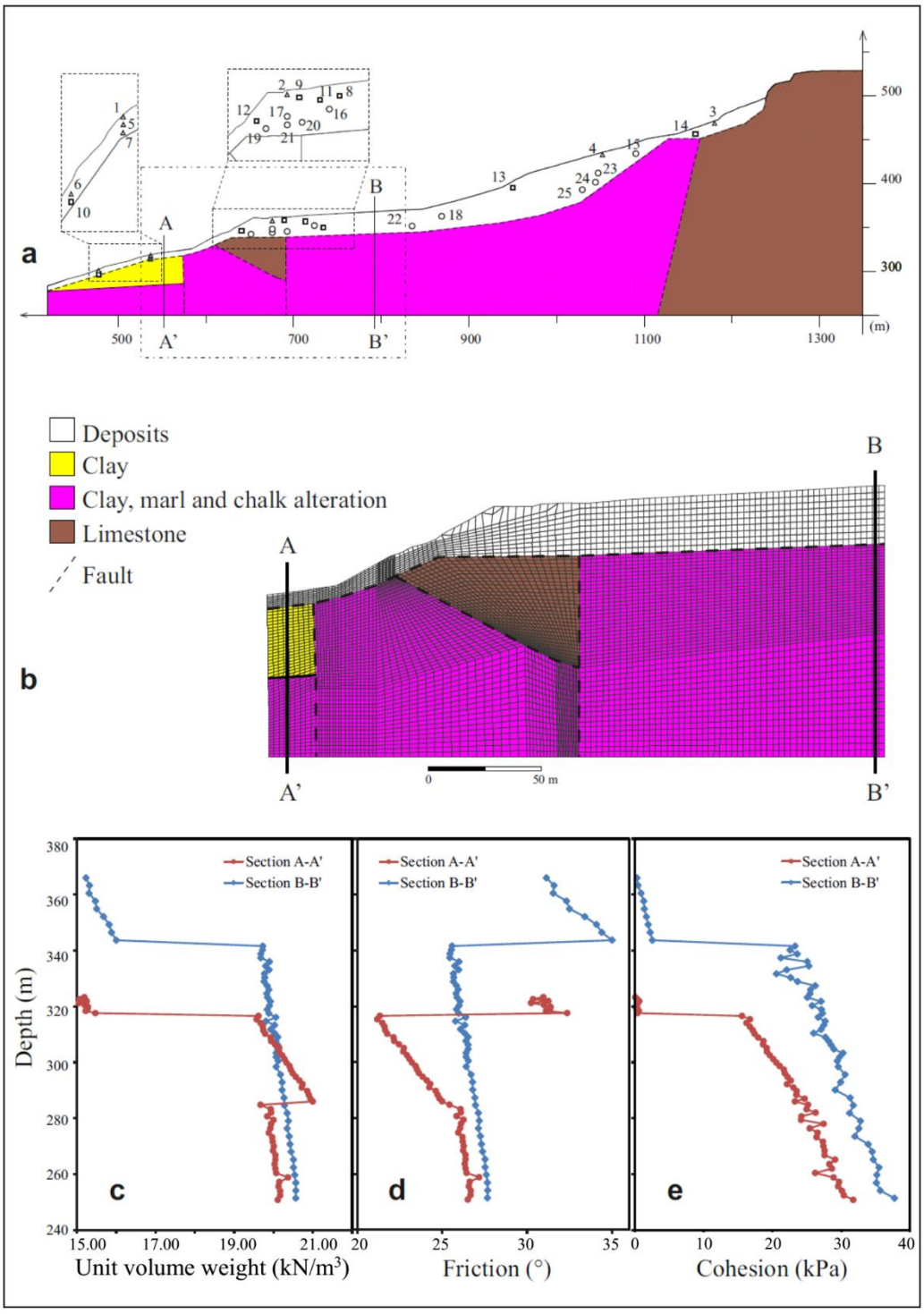

A specific type of grid was selected (Fig. 6b), suitable for discretizing the soil with small mesh sizes and including existing discontinuities. The Mohr-Coulomb parameters for all materials are indicated in Table 1. Fixed mean values were used for limestone, while variable parameters were employed for other materials according to the above discussed equations, as we can see in Fig. 6c, d, e, where the

graphs show some parameter variations with depth along two verticals A-A' and B-B'(Fig. 6b). The Yielding Index F_{YI} was calculated in each grid cell belonging to deposits formation. In order to study the influence of the uncertain knowledge of the selected distribution of physical-mechanical parameters on the local material stability (and integrity) of slopes, the stress state distributions consequent to the 650 realizations were acquired.

Table 1

Mechanical parameters for each material.

	Unit volume weight (kN/m^3)	Friction (°)	Cohesion (kPa)	Elastic modulus (MPa)
Deposits	15.00 ÷ 17.00	30 ÷ 40	0 ÷ 5	3 ÷ 4
Clay	19.50 ÷ 21.00	21 ÷ 25	15 ÷ 25	10 ÷ 15
Clay, marl and chalk alteration	19.50 ÷ 21.50	25 ÷ 30	20 ÷ 50	25 ÷ 40
Limestone	24.00	40	50	100

At the end of each analysis, two particular FISH functions were employed, both related to each grid cell. The first, *ps3d.fis*, allowed calculating the principal stress and record them in an appropriate extra grid variables, the second, *mcfos.fis*, was used to calculate F_{YI} factor, based on the calculated values of the stress and on physical-mechanical parameters. However, in order to conveniently discuss the set of the results also from a statistical point of view, we grouped (by FISH and Fortran routines not reported) the whole ensemble of the F_{YI} – resulting from the 650 Monte Carlo multiple realizations and related to the 2943 meshes of the deposits formations – into different size unit intervals, called bins in the histogram rendering. In Fig. 7, the distribution of F_{YI} resulting from two different Monte Carlo realizations, with 0.25 size interval increments, are displayed. It is worth noting that the F_{YI} variability of certain areas is lower than the variability of other areas, as the more detailed discussion reported in the following section will confirm.

Fig. 7. F_{YI} distribution in the deposits formations, 0.25 unit interval increments.

4. Statistical analysis

The resulting F_{YI} numerical ensembles are analyzed by a statistical point of view. To this purpose, some commonly utilized tools were selected and briefly described in Table A.1 (Appendix).

4.1. Global statistics insights

For each of the 650 different realizations, the number of spatial meshes, each of which associated to a small area, whose F_{YI} values were within a unit interval range around a selected mean, was counted. Fig. 8a shows the resulting distributions and the variation of the percentage of the total meshes of the deposits formations, grouped into 12 ensembles characterized by 0.25 unit interval increments starting from F_{YI}=1.125. The inspection of Fig. 8a, suggested the introduction of two more parameters. The first one was a Coefficient of Variability (COV, as named in statistics) and accordingly defined as: $\varepsilon_r = \Delta/\mu$, where Δ was the total variation of the percentages of the number of meshes (the vertical bar length in Fig. 8a) counted for each of the 12 ensembles, while μ was the mean value of the meshes number percentages counted over the 650 realizations. The other one was the median difference defined as: $(M_{var\_distr} - \mu)$, where $M_{var\_distr} = (Max + Min)/2$, while 'Max' and 'Min' were, respectively, the upper and the lower values of each bar in Fig. 8a.

Fig. 8. a) Total distributions, 0.25 unit increment (F_{YI} = 1.125 as first value); b) Relative variability and median difference of meshes number within F_{YI} unit.

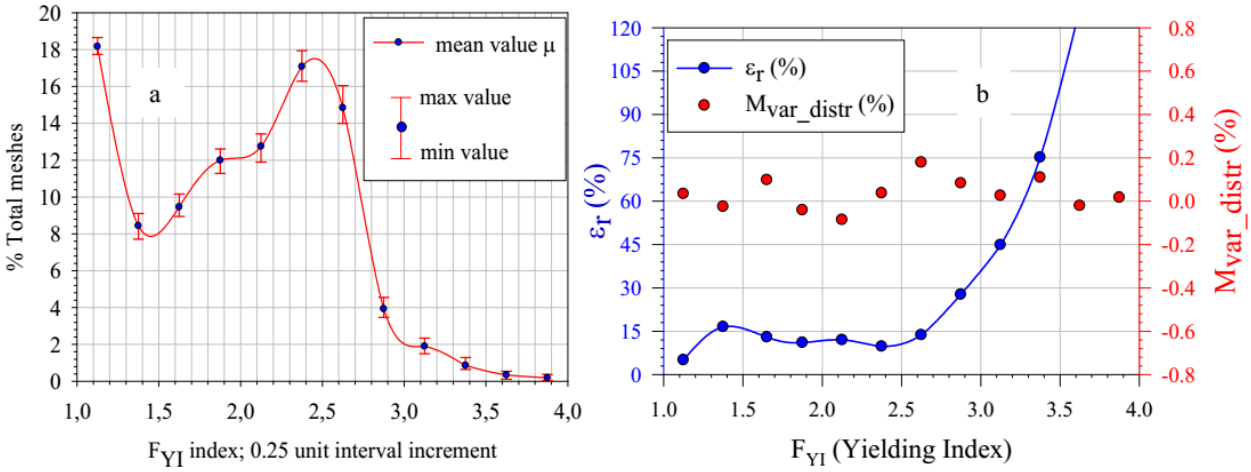

Accordingly, the ε_r indicates how many areas, in percentage, changed their stress state when parameter values changed, in other words the sensitivity of areas stress state to the overall parameters variability, while M_{var_distr} is a heuristic indication of the skewness of the distribution of the number of meshes, characterized by a F_{YI} value. Thus, in Fig. 8b the relations between ε_r and M_{var_distr} vs F_{YI} are reported. It appears that the relative variability ε_r is correlated in some way to the F_{YI} index value, while the relation between the skewness and the index seems to be completely random. Observing the ε_r values, it appears that the relative variability of the meshes number, in some sense also connected to the resulting variability of areas characterized by a specific stress state, is much lower when the area stress state is close to critical conditions. Moreover, the trend of the ε_r parameter identifies three different F_{YI} fields: the first ranging from 1 to 1.45, the second from 1.45 to 2.5 and the last one from 2.5 to 4 (in the figure, F_{YI} values greater than 3.5 are out of the selected scale). In the first and last fields, where the stress state is respectively close to or far from critical conditions, the area extension affected by changing condition increases as the F_{YI} increases, while within the intermediate fields the relative extension variability is almost unaffected by the increase of Yielding Index. All this, at least, according to the selected mathematical models.

4.2. Local statistics insights

Previously, a global investigation was performed. An explorative analysis is performed about the issue of how the stress state related to some areas of the deposit layer was influenced by the uncertain knowledge of the numerical values of the most important mechanical parameters. To this end, 25

nodes, representative as much as possible of each critical region of the layer, labelled according to their progressive distance from the topographic line (depth) (Fig. 6a), were selected by inspecting Figs 6, 7. As far as possible, all meshes typologies and zones, through the superficial deposit, were identified and represented by one or more nodes.

An important explored parameter, required for comparing data, was the 'Mean' value of the statistical ensembles. In Fig. 9, the related comparisons are displayed. In this case, non-vanishing correlations seem to emerge between the Standard deviation (Fig. 9a, $R^2 = 0.6131$), the Kurtosis (Fig. 9b, Squared Pearson Correlation: $R^2 = 0.8035$), the Skewness (Fig. 9c, $R^2 = 0.6081$) and the Mean. On the other hand the COV parameter is clearly uncorrelated to the Mean (Fig. 9d).

Fig. 9. Sigma, Kurtosis, Skewness, COV vs mean.

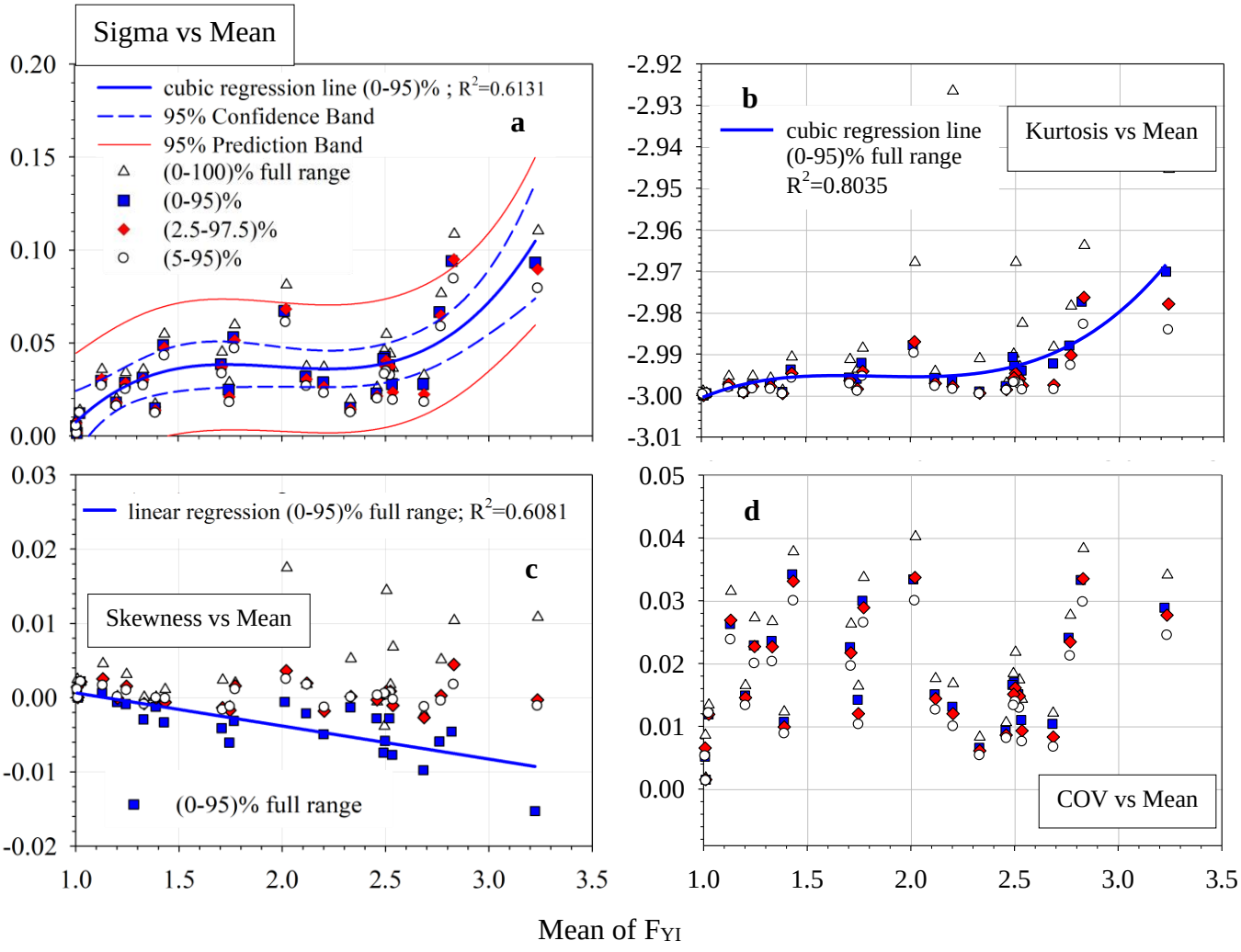

The resulting fitting curves were selected according to the requirement of the best goodness of fit. In Fig. 9a, it is interesting to observe that the cubic regression line of the comparison of the Standard deviation $\sigma_{\Delta R2}$ (regarding only th F_{YI} values falling within the 0.% up to 95% percentile, Table A.1,

Appendix) to the mean $\mu_{\Delta R2}$ (values ranging within the interval 0-95%) is similar to the regression line of the parameter ε_r in Fig. 8b. Moreover, we grouped the 25 nodes, displayed in Fig. 6a, into three sets, characterized roughly by different depths and positions: superficial nodes numbered from 1 to 7, depth ranging from 0.11 to 3.85 m; intermediate nodes from 8 to 14, depth from 4.16 to 6.81m; deep nodes from 15 to 25, depth from 11.90 to 35.53 m. In Table A3, the comparison between Standard deviations to Means, related to different percentiles range, in order to avoid outliers, are indicated. Also in this case, after many attempts aimed at identifying correlations trend, the 0%-95% percentiles range was selected to perform and discuss further analyses (in particular, $\mu_{\Delta R2}$ and $\sigma_{\Delta R2}$ in bold characters in Table A3. Accordingly, hereafter only the 0%-95% percentiles range will be considered. The results are reported in Fig. 10.

Fig. 10. Sigma, Kurtosis, Skewness, COV vs Mean.

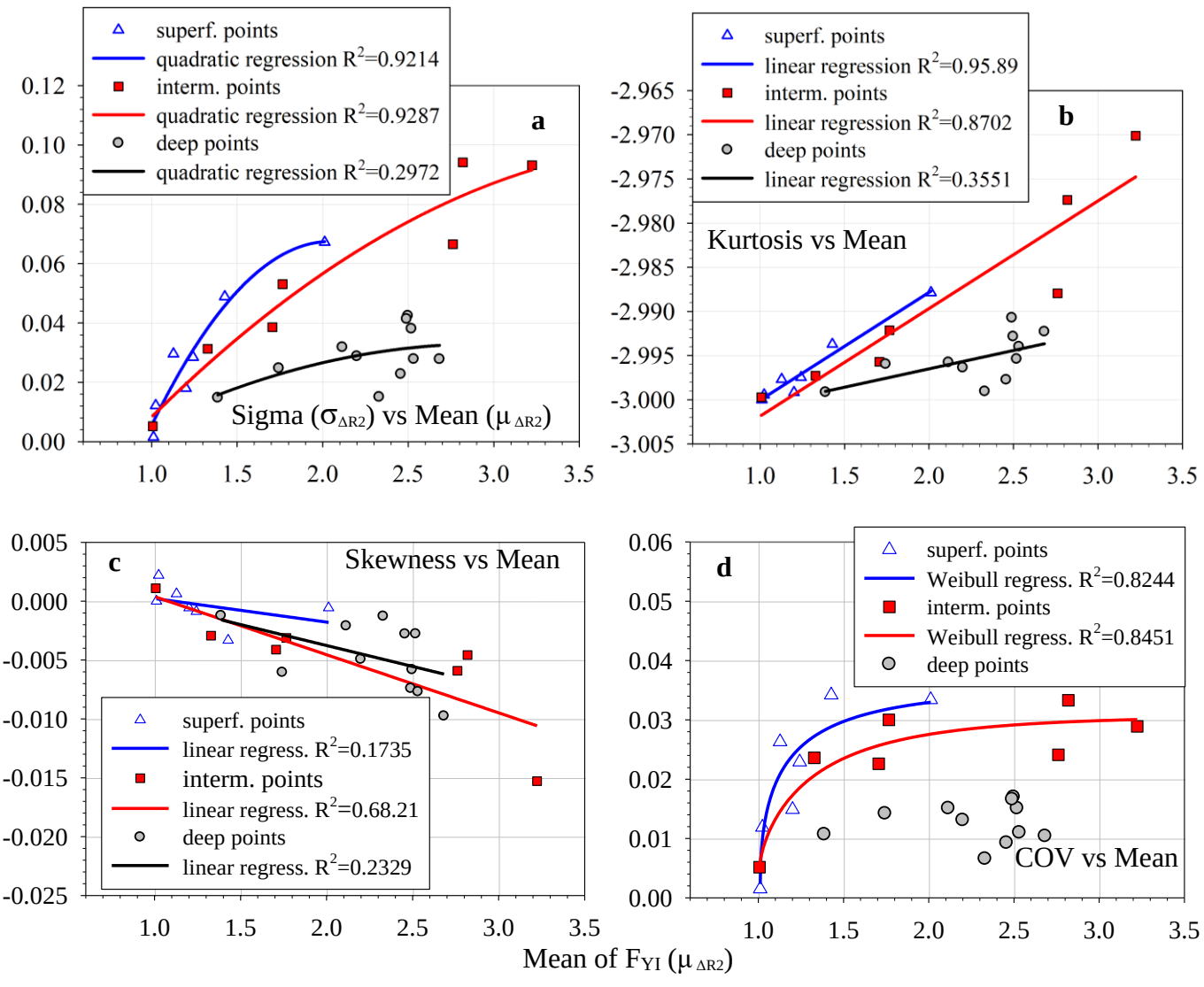

It appears clearly that for superficial and intermediate points, located within the first 7 m, strong correlations between the Standard deviation (quadratic), Kurtosis (linear) and the Mean take place. The related R^2 ranges between 0.8702 and 0.9287. The correlation between the COV and the Mean is described by a Weibull fitting curve ($0.8244 < R^2 < 0.845$), indicating that just for low F_{YI} values the two parameters are correlated. The Skewness is only weakly correlated to the Mean ($0.1735 < R^2 < 0.6821$). On the other hand, regarding nodes located in the third layer (depth higher than 7-12 m), these kinds of correlations become low or are completely lost. A statistical computer code (STATGRAPHICS Centurion XVI, 2010) was applied in order to analyse to what extent the initial distributions of the numerical values, fitting the mechanical parameters input, are comparable with the distributions of the numerical F_{YI} values resulting from the application of the mathematical model discussed in the previous sections. The option called *Comparison of Alternative Distributions* on the *Tables and Graphs* dialog box allows to select, among the 27 most common distributions, the best curves fitting the data under study and to list them according to their goodness of fit, in accordance with the 'Maximum LogLikelihood Test' (MLLT) (Cox and Hinkley, 1974, Casella and Berger, 2001). Tables A.4a and 4b report the results of the tests aimed at identifying the goodness of fit, related to the statistical comparison of the cohesion coefficients distributions inputs and the resulting F_{YI} distributions, for the selected nodes. The higher the value of the number along the columns, the better the goodness of fit to data of the selected distributions.

For each node, bold blue and red colours indicate the numerical rank of the best fitting, respectively, of the cohesion coefficients and the resulting F_{YI} selected distributions. In order to gain more insights on the sensitivity of the resulting F_{YI} numerical values and of their distributions with respect to the uncertainties associated with the cohesion coefficient (the selected parameter in order to study this kind of issue), we detailed the performed analysis, reporting the related graphics of some selected nodes, representative of particular areas of the slope under study (Figs. 11-15). In the figures, the blue colour of the F_{YI} fitting curves indicates the same fitting distribution as that of the cohesion coefficient, identified by MLLT, while the red colour indicates the best fitting curves of the F_{YI} values ensemble, resulting from the 650 runs, identified by the same MLLT procedure. Since each distribution was elaborated starting from the Standard Normal Distribution, a 'Normality' test was also included to visualize how the geo-mechanical, the mathematical and the numerical (in particular the discretization of the continuum through meshes) selected models could modify the final resulting distributions. Moreover, it is worth noting that, according to the initial assumption that excludes (for this step) any connectivity among the geo-mechanical parameters distributions of nodes, the distributions of the cohesion coefficient of each node is completely independent from the others.

Fig. 11. Comparison between cohesion coefficients and F_{YI} fitting distributions related to superficial nodes 1, 2, 3, 4.

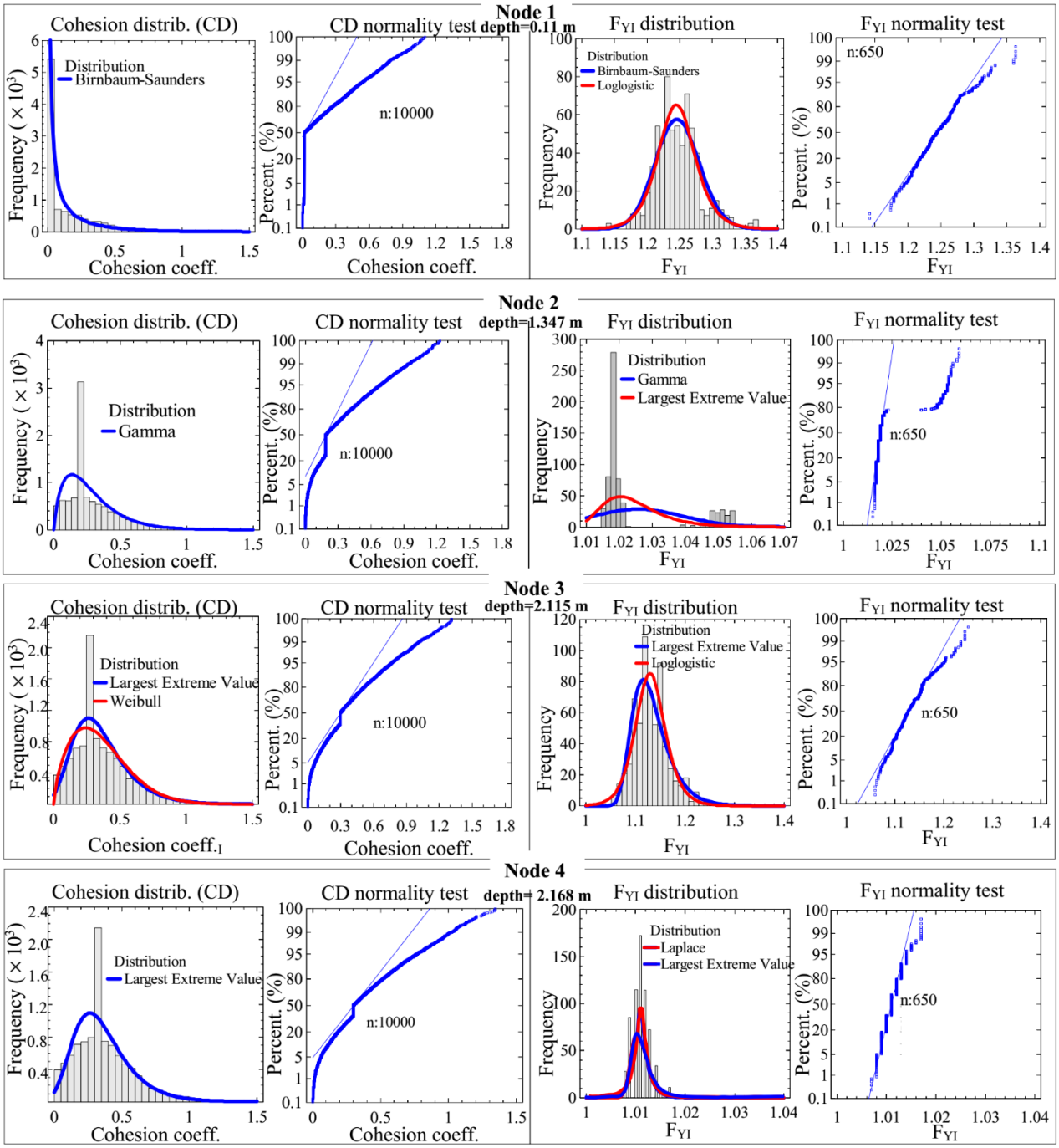

On the other hand, the distributions of the resulting F_{YI} coefficients may be affected not only by the local features of the selected area, but also, and in a very complicate way, by the influence of the entire system, at different scales. By consequence, the comparison of these two kinds of distributions could be considered as an indication of how the uncertainties were transmitted (according to the selected geological-mathematical and numerical models) through the system and which are the areas more sensitive to the lack of knowledge of fundamental parameters, necessary to run the model. First

of all, we considered (Fig. 11) the superficial nodes 1, 2, 3 and 4, whose depths range from 0.11 m to 2.168 m (Fig. 8a). The 'Normality' test failed for all the resulting distributions related to the implemented cohesion coefficient input distribution, indicating that – for these selected nodes – the application of the mathematical model strongly affected and perturbed the Standard Normal Distribution on which the Monte Carlo approach was based (Fig. 2b and c). In particular, for the Cohesion coefficient, the observed jump of the 'Normality' test curve and spike, if any, are a consequence of setting a random outlier value, resulting from Eq. (3) and (7), equal to the distribution mean (section 2). F_{YI} 'Normality' tests for nodes 1, 3 and 4 are verified for central data, but not for the tails. For node 2 the test failed completely. For these superficial nodes, the fitting F_{YI} distributions are completely different compared to the cohesion coefficient distribution. As regards these nodes, it could be inferred that the obtained F_{YI} distributions were strongly affected by non-local 'transmission' of the uncertainties that modified the local distribution of the assigned inputs parameters. In particular, node 1 is located at the toe of the slope (Fig. 8a), while node 2 (Fig. 8b) is located in an area that was discretized differently from the neighbouring regions. This occurrence could affect the outcomes of the models. Moreover, the resulting F_{YI} distribution of node 2, clearly indicates that the related area presents a criticality by a stability point of view.

Fig. 12. Comparison between cohesion coefficients and F_{YI} fitting distributions related to superficial nodes 5, 6.

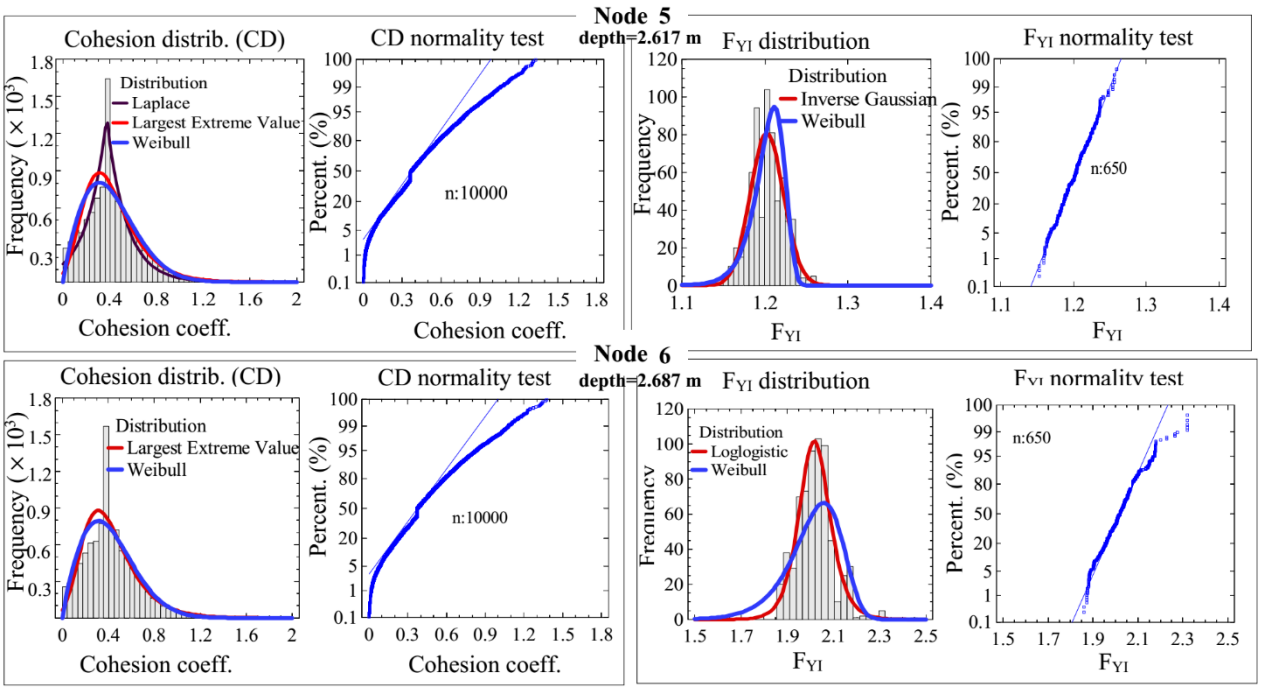

Furthermore, the spreading of its distribution appears to be low. It is interesting that, despite the proximity of node 5 to node 1 (Fig. 6a) and the similarity of the related meshes (Fig. 6b), the two kinds of distributions and the resulting 'Normality' tests are different (Fig. 12). The only difference is the depth of their locations. Accordingly, it could be inferred that, at the toe of the slope, also a relative difference in the depth (about 2.5 m) could be significant. Node 6 is located at a different point of the toe, but at almost the same depth of the node 5 (2.687 m). For both nodes the cohesion coefficient distributions were the same (Weibull), but their F_{YI} distributions were different, indicating that there may be a different influence of the entire system on the two different meshes. Fig. 13 shows, in particular, the response of the intermediate node 12 that appears to be similar (except for the occurrence of a double mode distribution regarding the node 2) to both the distribution and the resulting 'Normality' test of node 2.

Fig. 13. Comparison between cohesion coefficients and F_{YI} fitting distributions related to intermediate nodes 9, 12.

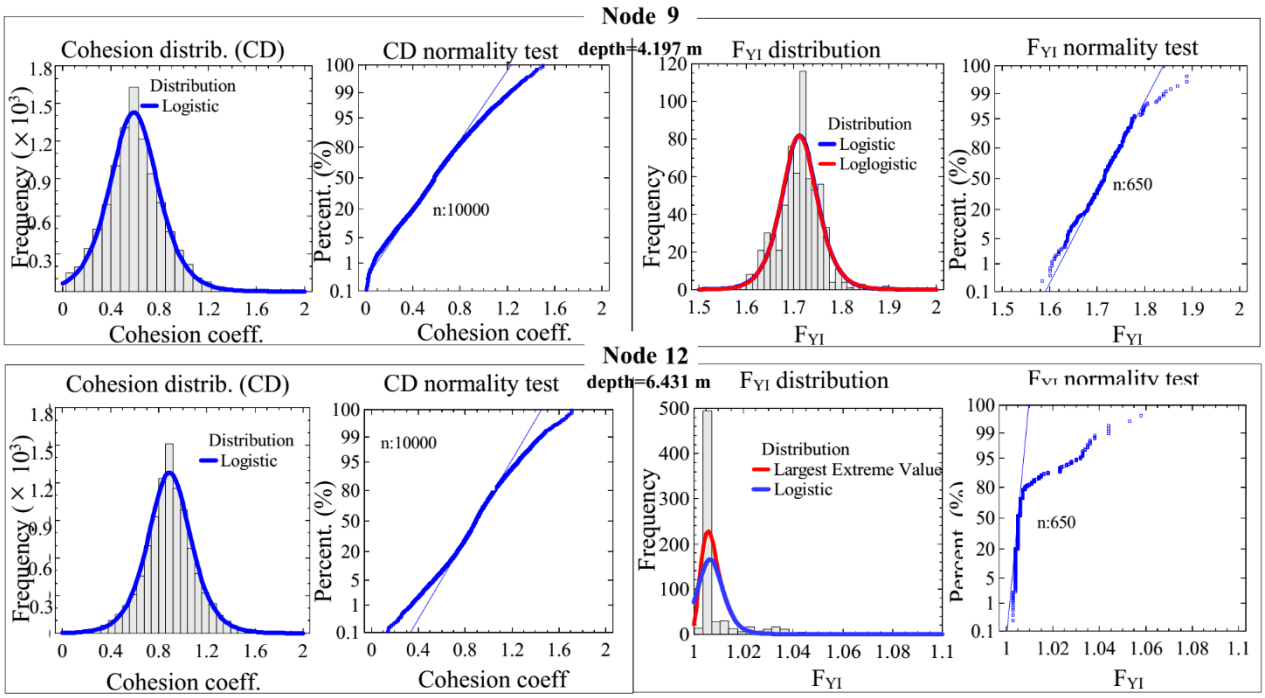

Further, the node 12 experiences low values of both the mean and the spreading of its resulting F_{YI} distribution. It is interesting to note that both nodes 2 and 12 are located in an area that, reasonably, could be considered critical by a global stability of view. Nevertheless, also the mean and the spreading of node 4 are low. However, it does not seem to be located in a critical region of the slope (Fig. 6a). Accordingly, the particular response of the F_{YI} distribution could be ascribed to the occurrence of just local instability, not necessarily due to an actual phenomena, but also to the applied

model. Moreover, node 9, although located in an area close to node 2, thus with the same type of discretization, did not experience the same F_{YI} distribution characteristics. We can deduce that stability conditions, in this case, are more influential than the type of the selected mesh. Finally, in Figs 14 and 15, the responses of an intermediate node (14) and deep nodes (15, 19, 23, 24, 25).

Fig. 14. Comparison between cohesion coefficients and F_{YI} fitting distributions related to intermediate node 14 and deep nodes 15, 19.

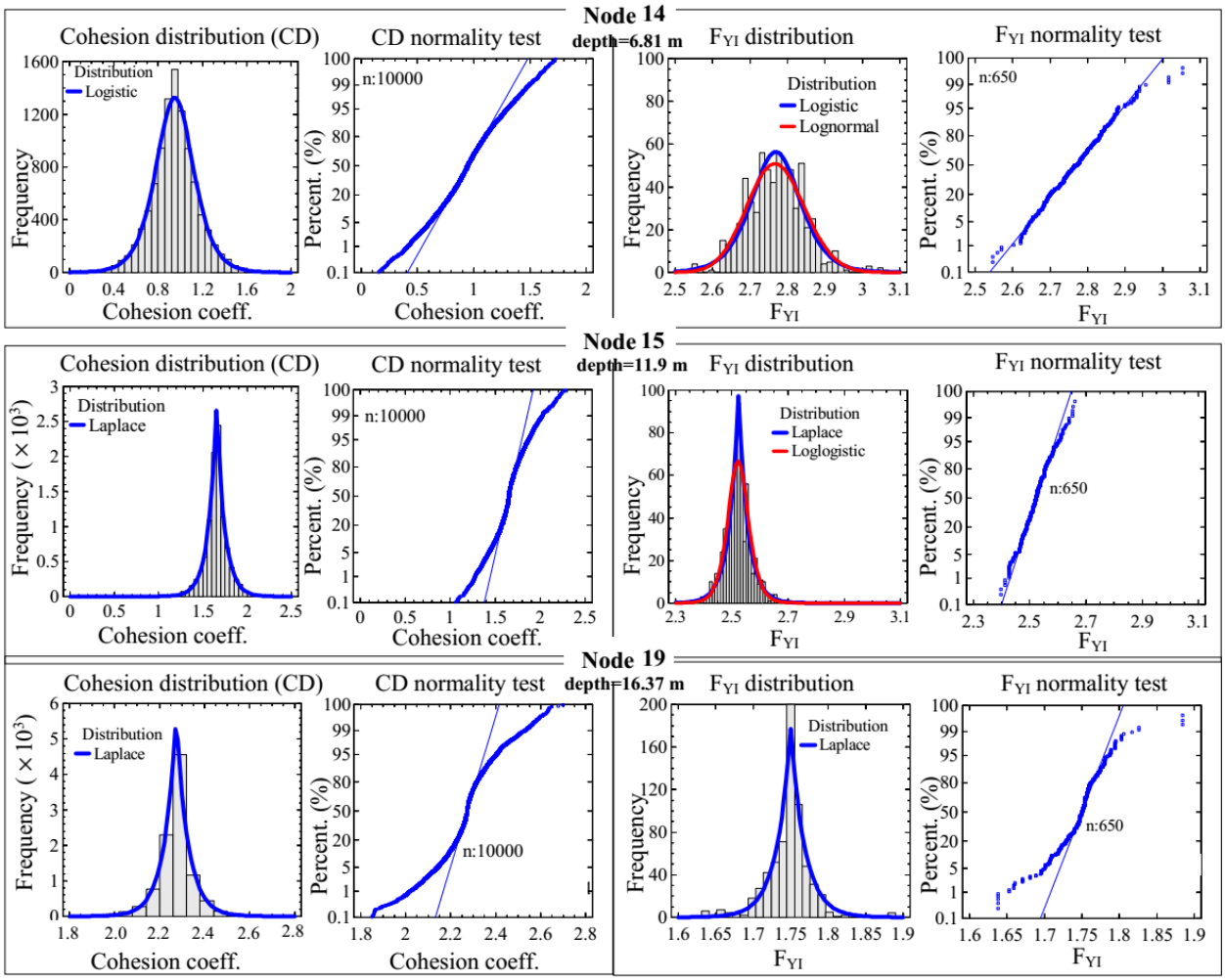

Based on the previous discussion, since the F_{YI} distribution is very similar to the correspondent cohesion coefficient, all these nodes, except for the last one, node 25, appear to be weakly influenced by the global response of the system. Node 25 was placed at the point where the distance from the corresponding topographic is maximum for the selected region of the slope. Therefore, similarly to what happens for node 1, the particular selected mathematical model (based on a linear increase of the mechanical coefficients as the depth increases, eq. 6) strongly affected the resulting cohesion coefficient. However, it is interesting to note that the resulting F_{YI} distribution (also for node 1, but in particular for node 25) is completely different. In addition, by observing the answer of other similar points, 23, 24, 25, this occurrence suggests that, in this case, the spatial scale of the 'influence area'

(in which the mechanical response of each node is related to that of the other nodes) is medium, that is, non-local (single mesh), non-global (the whole system) but includes a limited number of meshes.

Fig. 15. Comparison between cohesion coefficients and F_{YI} fitting distributions related to deep nodes 23, 24, 25.

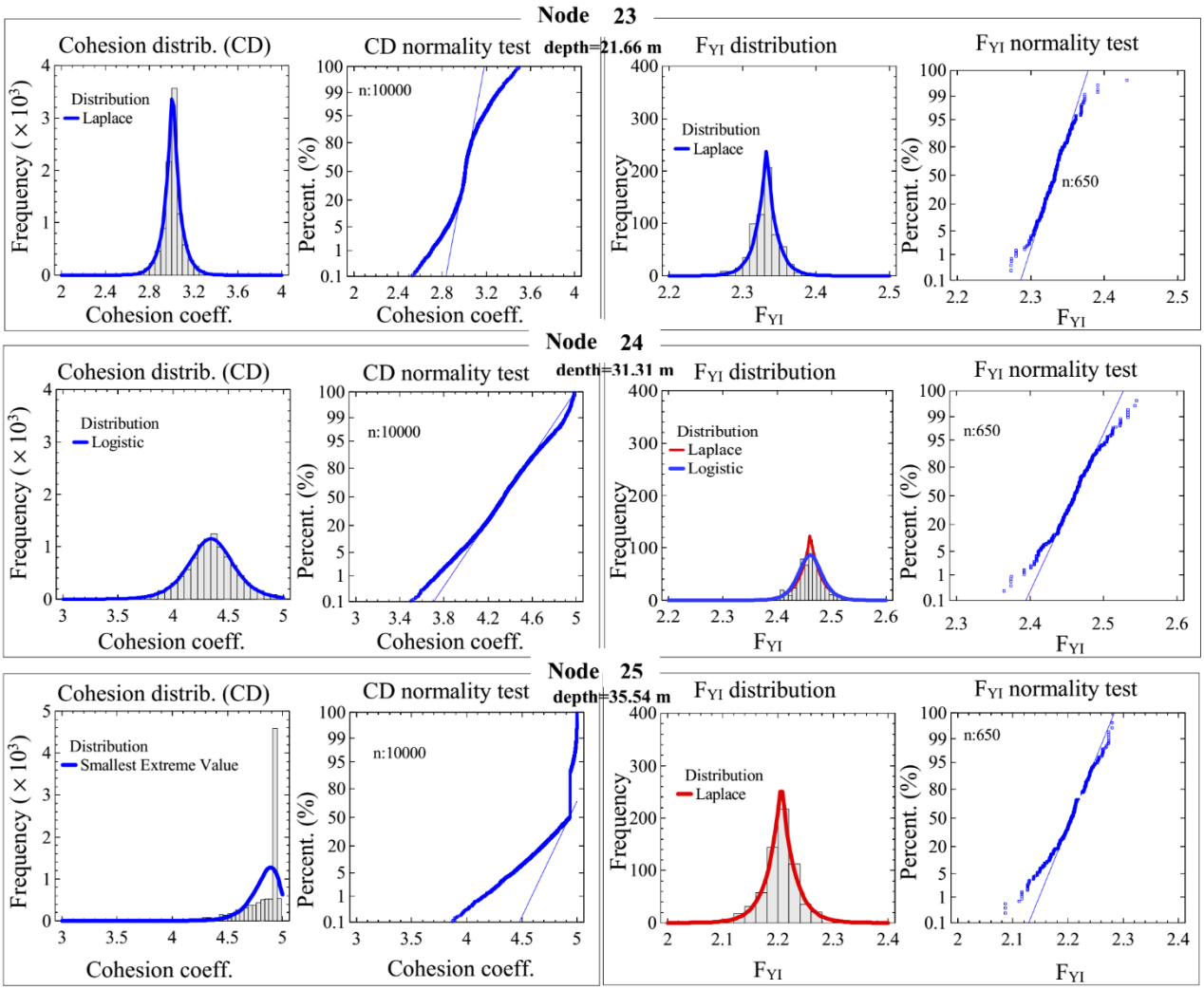

In summary, observing the previous figures (Figs. 11-15) and in particular Table A.4a and b fitting ranks, we can infer that as regards superficial nodes (0.11m - 3.85m; 1-7 nodes) the resulting F_{YI} distributions is different to the cohesion coefficient distributions (the blue and red fitting ranks are not within the same columns under the same fitting distribution), except for node 3, evidencing that the mechanical local response (single mesh) is strongly influenced by different spatial scales (medium up to large, thus more than few meshes). The same applies to intermediate nodes (4.16m - 6.81m; 8 - 14 nodes), except node 9. On the other hand, with respect to deep nodes (11.90m - 35.54m; 15-25 nodes), similar distributions, Laplace fitting curve, are observed for seven nodes with the exception of 4 nodes (15, 20, 24, 25).

5. Conclusions

In this paper, the statistics of the numerical stress states resulting from different realizations of as realistic as possible mathematical model of an actual slope, characterized by heterogeneity at multiple scales, is presented and discussed, in order to study uncertainties propagation within the selected system. To make the analyses as simple as possible, we considered the selected test case in a dry condition, avoiding considerations about the saturation state of the system. The spatial distribution of physical-mechanical parameters was realized **by** random Monte Carlo assignment to each point of a numerical value belonging to a probabilistic distribution ensemble, assumed valid for the system under study, added to a trend along the depth, identified by mechanical, physical and geotechnical considerations.

Compared to previous approaches adopted also by us, instead of identifying a global and unique safety factor through degradation of mechanical parameters until rupture, in this paper we focused on the Yielding Index F_{YI}, which can serve as a proxy for identifying a local stress state, approaching unitary value when close to local rupture conditions. This type of index can allow the identification of areas particularly susceptible to becoming locally unstable and which may also induce global instabilities. The numerical evaluation of this parameter depends on how the numerical model is performed, including also the treatment of the intrinsic uncertainties. However, the initial local assignment of a selected uncertainty could be heavily affected by the mechanical influence of the entire system. Accordingly, in this paper we proposed an approach to analyze how the variability and uncertainties propagate within the system under study, in order to identify zones where the uncertainties related to instability parameters may grow beyond the initial assignment.

The proposed algorithms were successfully implemented in a commercial code (FLAC2D) through an interactive tool (FISH) and then applied to an actual site as test case, with particularly complex lithostratigraphic characteristics. The discussed procedure and results highlighted the effectiveness and flexibility of the implementation. The analysis of the resulting statistical ensemble of the F_{YI} outcomes, related to twenty five nodes located in different places of the test slope and grouped into three levels, selected on the basis of their distances from the vertical point located on the topographic, seems to reveal, for superficial and intermediate levels (0.11m - 7m), an interesting correlation between the spreading of such parameters and their mean values (Fig. 10a). In particular, it appears that the variability, indicated in Fig. 10a as Sigma $\sigma_{\Delta R2}$ of the calculated F_{YI}, decreases as the value of the F_{YI} mean, obtained for each mesh by the calculations discussed above (Mean $\mu_{\Delta R2}$ in Fig. 10a), decreases. Thus, it appears that this kind of analysis indicates lack sensitivity to overall variability of the parameters affecting the mechanical response of superficial and intermediate layers zones (Fig. 10a) whose stress state is close to local stability criticality, at least from the particular typology of the

test case and the selected models. Namely, for the selected mathematical model and test case, when the local area under study is close to critical conditions, thus with low F_{YI} values, the probable statistical stress state distributions, resulting from multiple realizations of realistic set of numerical values of parameters, is less sensitive to the randomness of the available information; whereas, when the area is far from criticality, thus more stable, its stress state is more dependent on randomness. In a thermodynamics and entropic sense, it may be argued that since close to criticality just few states are accessible (low variability of the calculated F_{YI} coefficients), accordingly, the system is more 'ordinate', by a statistical point of view, than in stable conditions in which the number of ways to be stable is higher (high F_{YI} variability). Moreover, the comparison between the resulting F_{YI} distribution and the cohesion coefficient input, selected as an important mechanical parameter to which performing the comparison, suggests that some areas of the slope may be more influenced than others by what happens in more or less far areas, identifying a spatial connectivity and uncertainties transmission through local, medium and global scale of influence (Figs. 11-15).

The test slope system can be considered as common in engineering geology practice and, therefore, the proposed methodology can provide useful indications for similar or also different situations, in identifying areas of actual systems where any additional experimental surveys and more accurate numerical modelling could be focused, excluding less important zones by the above discussed point of view, saving time and economical efforts, important issues even for practitioners.

Acknowledgment

The authors would like to thank three anonymous referees and the Editor for the suggestions that helped to improve the clarity and the quality of the paper.

References

Andrade, J.E., Baker, J.W., Ellison, K.C., 2008. Random porosity fields and their influence on the stability of granular media. International Journal for Numerical and Analytical Methods in Geomechanics, 32, pp. 1147-1172.

J. Banks, J. S. Carson II, B. L. Nelson, D. M. Nicol, 2005. Discrete-Event System Simulation, Prentice Hall.

Box, G.E.P. and Muller, M.E., 1958. A note on generation of random normal deviates. Ann. Math. Statist., 29, pp. 610-611.

Bossi, G., Borgatti, L., Gottardi, G., Marcato, G., 2016. The Boolean Stochastic Generation method -BoSG: A tool for the analysis of the error associated with the simplification of the stratigraphy in geo-technical models. Engineering Geology, 2013, 99-106.

Calista, M., Pasculli, A., Sciarra, N., 2015a. Reconstruction of the geotechnical model considering random parameters distributions. Engineering Geology for Society and Territory Vol. 2: Landslide processes pp. 1347-1351. doi: 10.1007/978-3-319-09057-3_237; ISBN: 978-331909057-3; SCOPUS id: 2-s2.0-84944628353.

Calista, M., Miccadei, E., Pasculli, A., Piacentini, T., Sciarra, M., Sciarra. N., 2015b. First results of morphometric analysis, multitemporal geomorphological investigation and numerical modeling of the Montebello sul Sangro landslide (Abruzzo, Central Italy). Rendiconti Online Societa Geologica Italiana 13, 307–310. doi: 10.3301/ROL.2015.127; ISSN: 20358008; WOS: 000373173500079; SCOPUS id: 2-s2.0-84930718363.

Calista., M., Miccadei, E., Pasculli, A., Piacentini, T., Sciarra, M., Sciarra, N., 2016. Geomorphological features of the Montebello sul Sangro large landslide (Abruzzo, Central Italy). J. Maps 12 (5), 882–891. doi: 10.1080/ 17445647.2015.1095134; ISSN: 17445647; WOS: 000389542600021; SCOPUS id: 2-s2.0-84944909158.

Casella, G., Berger, R., 2001. Statistical Inference. Second Edition Duxbury Advanced Series, ISBN 0-534-24312-6, pp. 686.

Ching, J., Wang, J.S., 2016. Application of the transitional Markov chain Monte Carlo algorithm to probabilistic site characterization. Engineering Geology, 203, 151-167

Cox, D.R., Hinkley, D.V., 1974. Theoretical Statistics. Chapman and Hall. Springer ISBN 0-412-12420-3, pp.522.

Esposito, L., Esposito, A.W., Pasculli, A., Sciarra, N., 2013. Particular features of the physicaland mechanical characteristics of certain Phlegraean pyroclastic soils. CATENA, vol. 104,pp. 186-194. ISSN: 03418162; doi: 10.1016/j.catena.2012.11.009; WOS:000315556600019; SCOPUS id: 2-s2.0-84873130083.

Fenton, G.A. and Vanmarke, E.H., 1990. Simulation of Random Fields via Local Average Subdivision. ASCE J. Engrg. Mech. 116 (8), 1733-1749.

Ghanem, R.G., Spanos, P.D., 1991. Stochastic finite elements: A spectral approach. Springer, New York

Hamdia, K.M., Silani, M., Zhuang, X., He, P., Rabczuk, T., 2017. Stochastic analysis of the fracture toughness of polymeric nanonparticle composites using polynomial chaos expansions. International Journal of Fracture 206, 215-227.

Hesse, F., Prykhodko, V., Schluter, S., Attinger, S., 2014. Generating random fields with a truncated power-law variogram: A comparison of several numerical methods. Environmental Modelling & Software, 55, 32-48.

Itasca consulting group, inc., 2008. Flac version 6.0, Fast Lagrangian Analysis of Continua in three dimension. Minneapolis, USA.

James, F., 2006. Statistical Methods in Experimental Physics., 2nd Edition. World Scientific, pag. 345.

Jiang, J., Ehret, D., Xiang, W., Rhon, J., Huang, L., Yan, S., Bi, R., 2011. Numerical simulation of Qiaotou Landslide deformation caused by drawdown of the Three Gorges Reservoir, China. Environmental Earth Sciences, vol. 62, pp 411-419.

Minatti, L., Pasculli, A., 2010. Dam break Smoothed Particle Hydrodynamic modeling based on Riemann solvers. Advances in Fluid Mechanics VIII, WIT Transactions on Engineering Sciences; WIT Press 2010, ISSN 1743-3533, DOI: 10.2495/AFM100131; ISBN 978-1-84564-476-5; SCOPUS id: 2-s2.0-78449235684, Vol. 69, pp. 145-156.

Minatti, L., Pasculli, A., 2011. SPH numerical approach in modelling 2D muddy debris flow. 5th International Conference on Debris-Flow Hazards Mitigation Mechanics, 15-17 June 2011 DOI: 10.4408/IJEGE.2011-03.B-052, Casa Editrice Università La Sapienza Roma; ISBN 978-88-95814-46-9; ISSN 1825-6635; SCOPUS id: 2-s2.0-84861619060, pp. 467-475.

Pasculli, A. and Sciarra, N., 2002. A 2D Mathematical and Statistical Modelling of Soils Structures. In: Proceedings of 8th Annual Conference of the Int. Ass. for Mathematical Geology 2002. Berlin, Germany, 1, pp. 111-116.

Pasculli, A. and Sciarra, N., 2003. Nodalizzazione ed Interpolazione agli Elementi Finiti di Eterogeneità Strutturali in terreni granulari: Applicazione ai pendii (in Italian). Proceedings of 1th Conference of AIGA 2003. Chieti (Italy): Rendina Editor ISBN 88-86698-40-2, pp. 551-575.

Pasculli, A. and Sciarra, N., 2006a. A 3D landslide analyses with constant mechanical parameters compared with the results of a probabilistic approach assuming selected heterogeneities at different spatial scales. Giornale di Geologia Applicata, 3, pp. 269-280.

Pasculli, A., Calista, M., Mangifesta, M., 2006b. The effects of spatial variability of mechanical parameters on a 3D landslide study. 4th International FLAC Symposium on Numerical Modeling in Geomechanics 29-31 May 2006, Paper 01-05. Madrid (Spain): Itasca Consulting Group, Inc. Minneapolis, ISBN 0-9767577-0-2, pp. 1-8.

Pasculli, A., Minatti, L., Sciarra, N., Paris, E., 2013. SPH modeling of fast muddy debris flow:Numerical and experimental comparison of certain commonly utilized approaches. Italian Journal of Geosciences; ISSN: 20381719; DOI: 10.3301/IJG.2013.01; WOS:000326908600004; SCOPUS id: 2-s2.0-84886468697; Vol. 132, Issue 3, pp. 350-365.

Pasculli, A., Minatti, L., Sciarra, N., 2014. Insights on the application of some current SPH approaches for the study of muddy debris flow: Numerical and experimental comparison. Wit

Transaction on Information and Communication Technologies, 10th International Conference on Advances in Fluid Mechanics, AFM 2014; A Coruna; Spain; 1 July 2014 through 3 July 2014; ISSN: 17433533 ISBN: 978-184564790-2; DOI: 10.2495/AFM140011; SCOPUS id: 2-s2.0-84907611231; 82, 3–14.

Pasculli, A., Sciarra, N., Esposito, L., Esposito, A.W., 2017. Effects of wetting and drying cycles on mechanical properties of pyroclastic soils. CATENA, vol. 156, pp. 113-123.ISSN: 03418162 doi: 10.1016/j.catena.2017.04.004; SCOPUS id: 2-s2.0-85017109027.

Rabczuk T., Areias, P. M. A., 2006. A new approach for modelling slip lines in geological materials with cohesive models. International Journal for Numerical and Analytical Methods in Geomechanics, 30, 1159-1172.

Rabczuk T., Areias, P. M. A. and Belytschko, T., 2007. A simplified mesh-free method for shear bands with cohesive surfaces. International Journal for Numerical Methods in Engineering, 69, 993-1021.

Sciarra, N., Pasculli, A., Calista, M., 2006. The large Ancona landslide studies revisited including stochastical spatial variability of mechanical parameters. The 10th IAEG International Congress, Paper 8076-10 September 2006. Nottingham, United Kingdom: The Geological Society of London, pp. 1-11.

Sciarra, N., Calista, M., Miccadei, E., Pasculli, A., Piacentini, T., Sciarra, M., 2017. Morphometric Analysis, Multitemporal Geomorphological Investigation and Numerical Modelling of the Montebello sul Sangro Large Landslide (Abruzzo-Central Italy). Italian Journal of Engineering Geology and Environment, Special Issue 1, 117-133. doi: 10.4408/IJEGE.2017-01.S-11; SCOPUS id: 2-s2.0-85027508250.

Sitharam, T., G., Maji, V.B., Verma, A.K., 2007. Practical Equivalent Continuum Model for Simulation Jointed Rock Mass Using FLAC3D. Int. J. Geomech., 2007, 7(5): 389-395.

Snedecor, George W. and Cochran, William G., 1989. Statistical Methods. Eighth Edition, Iowa State University Press. ISBN 978-0-8138-1561-9.

STATGRAPHICS Centurion XVI homepage, 2010. http://www.stagraphics.com.

Sundell, J., Rosén, L., Norberg, T., Haaf, E., 2016. A probabilistic approach to soil layer and bedrock-levelmodeling for risk assessment of groundwater drawdown induced land subsidence. Engineering Geology 203, 126-139. .doi: org/10.1016/j.enggeo.2015.11.006.

Vanmarcke. E.H., 1977. Probabilistic modelling of soil profiles. Geotechnical Engineering, 103(11), 1227-1246.

Vu-Bac, N., Lahmer, T., Zhuang, X., Nguyen-Thoi, T., Rabczuk, T., 2016. A software framework for probabilistic sensitivity analysis for computationally expensive models. Advances in Engineering Software 100, 19-31.

Appendix

Fig. A.1. Flow Chart of the Numerical modelling

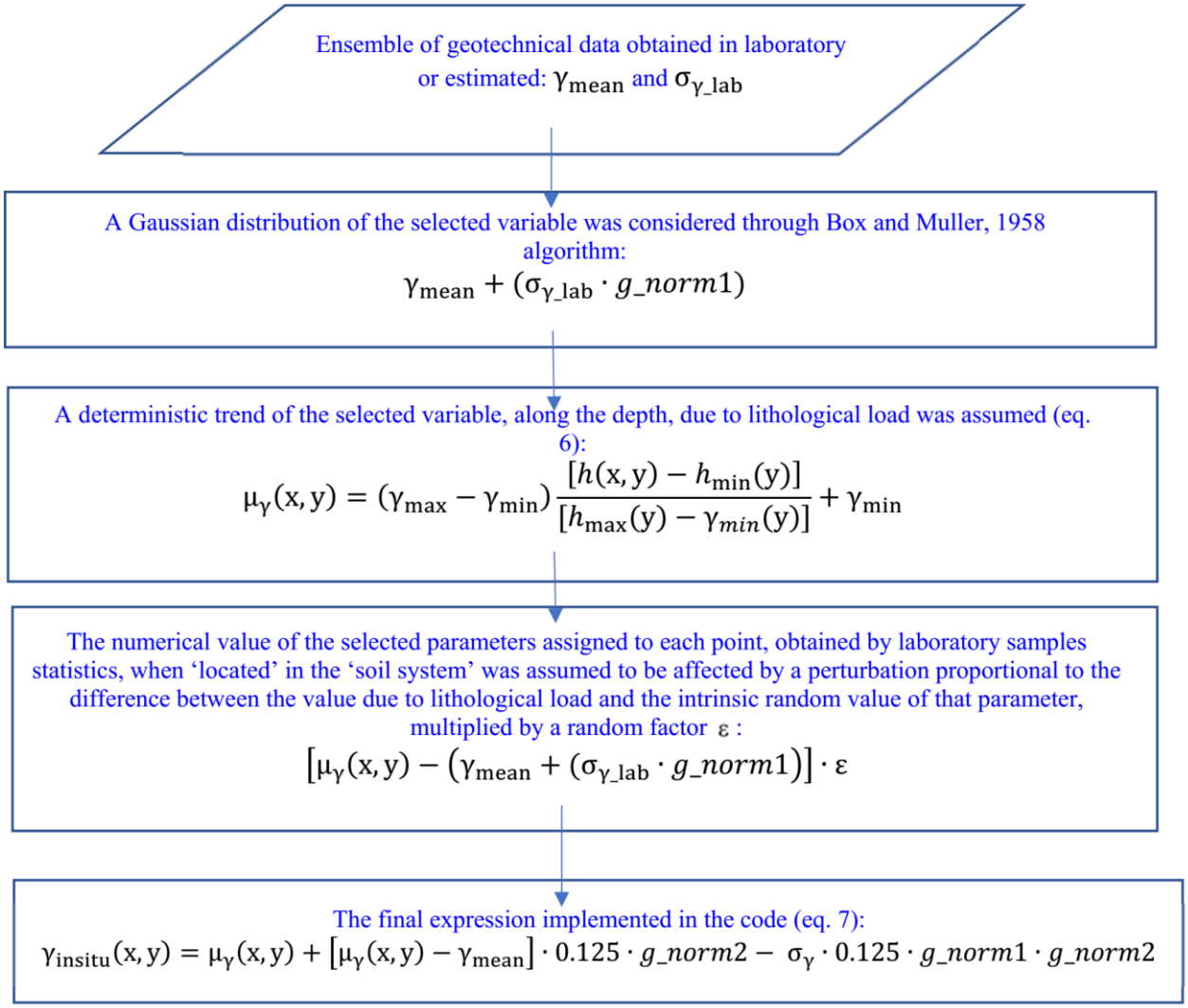

Fig. A.2. Explanatory figures of the adopted Monte Carlo model (eq.7): **a)** Numerical realization, through 7437 nodes, without a deterministic trend of the void distribution, regarding a synthetic2D slope section; **b)** Numerical realization, through 31408 nodes, with the lithological load of the void distribution; **c)** Uniform pseudo-random realization used for the Monte Carlo application; **d)** Void distribution along the section A-A'; **e)** Autocorrelation between a selected node and all the other nodes, showing no correlation (inside Bartlett's limit, Snedecor and Cochran, 1989 $|Autocorrelation| \leq \pm 1.96\sqrt{N}$ where N is the number of the considered points); **f)** Void distribution along the section A-A' related to the Fig. A.2.b; **g)** Void distribution along the section B-B' related to the Fig. A.2.b; **e)** Autocorrelation between a selected node and all the other nodes, showing correlation (outside Bartlett's limit) due to lithological applied trend; **i)** Numerical realization, through 31408 nodes, without a deterministic trend of the void distribution; **l)** Realization of a synthetic multilayer 2D section, characterized by faults an d weakness lines.

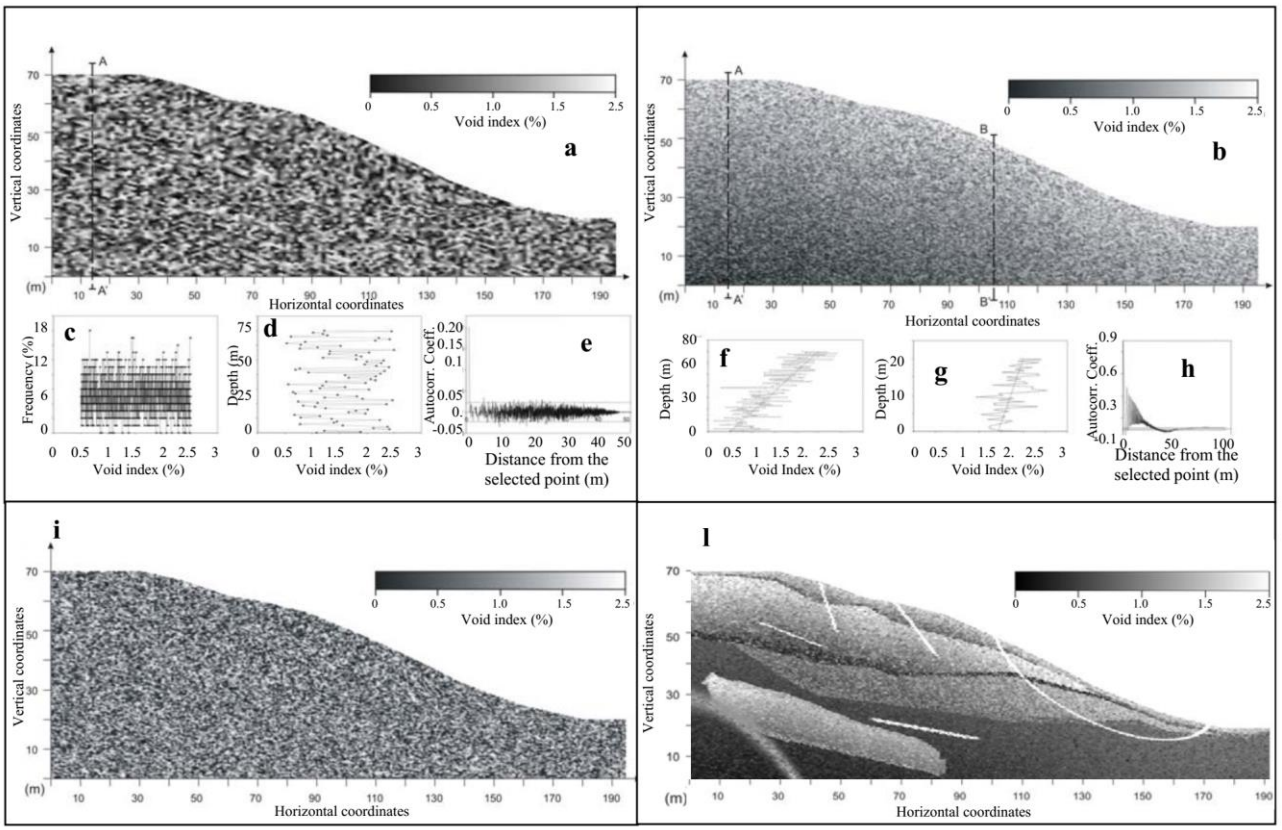

Fig. A.3a Distance from topographic FISH routine.

```
def distance
  var1=0.0
  var2=10000
  ;-------------------------------------------------------------
  loop i (1, izones)
    ;-----------------------------------------------------------
    loop j (1, jzones)
      yc = (y(i,j)+(y(i+1,j)+ y(i,j+1)+(y(i+1,j+1))/4.0
      ;yc = approximate centroid of the selected zone
      xx = x(i,j)
      yy = table(1,xx)
      zc =yy – yc
      ;zc = h(x,y) in Fig. 1
      hmax = max(zc, var1)
      ;hmax = hmax(x,y) in Fig. 1
      hmin = min(zc, var2)
      ;hmin = hmin(x,y) in Fig. 1
      var1=hmax
      var2=hmin
    end loop
    ;-----------------------------------------------------------
  end loop
  ;-------------------------------------------------------------
end
distance
```

Fig. A.3b Random density value realization FISH routine.

```
def property
  ;-------------------------------------------------------------
  loop i (1, izones)
    ;-----------------------------------------------------------
    loop j (1, jzones)
      rand1 = urand
      rand2 = urand
      rand3 = urand
      rand4 = urand
      dmax = 1700
      dmin  = 1500
      dmed = (dmax+ dmin)/2
      diff = dmax – dmin
      yc = (y(i,j)+(y(i+1,j)+ y(i,j+1)+(y(i+1,j+1))/4.0
      xx = x(i,j)
      yy = table(1,xx)
      zc =yy–yc
      g_norm1=((-2.*ln(rand1))^0.5)*cos(2.*pi*rand2)
      g_norm2=((-2.*ln(rand3))^0.5)*cos(2*pi*rand4)
      ;pi = p greek
      ;g_norm1, g_norm2: Box, Muller; Eq. (3)
      mu=((dmax-dmin)/(hmax-hmin))*(zc-hmin)+dmin
      ;mu = Eq.(6)
      phys=((dmin+dmax)/2+((dmax-dmin)/8.)*g_norm1
      ; phys = Eq.(1) and Eq.(2)
      density(i,j)=phys+[mu-phys]*[1+0.125*g_norm2]
      ; density(i,j)=Eq.(5), Eq.(6) and Eq.(7)
      ;-----------------------------
      if density(i,j)<dmin then
        density(i,j)=mu
      end if
      ;-----------------------------
      if density(i,j)>dmax then
        density(i,j)=mu
      end if
      ;-----------------------------
    end loop
    ;-----------------------------------------------------------
  end loop
  ;-------------------------------------------------------------
end
property
```

Table A.1 Exploited statistical tools

Name	Mathematical expressions	Notes
n		Number of realizations (650)
median		F_{YI} value corresponding to 50% percentage of the cumulative distribution function
Cumul(·)		F_{YI} value corresponding to the percentage equal to the value included in the brackets (·) of the cumulative distribution function
$\Delta R1$=	Ensembles embedding only the F_{YI} values falling within the following ranges: [Cumul(100.%), Cumul(0.0%)]	Suffixes used in Table A.3
$\Delta R2$=	[Cumul(95.0%), Cumul(0.0%)]	
$\Delta R3$=	[Cumul(97.5%), Cumul(2.5%)]	
$\Delta R4$=	[Cumul(95.0%), Cumul(2.5%)]	
Sample moment of *r-th* order	$m_r = \frac{1}{n}\sum_{i=0}^{n}(x_i - \hat{\mu})^r$	Statistical central moment about the mean: $\mu = \frac{1}{650}\sum_{i=1}^{650}(F_{YI})_i$
Standard Deviation	$\hat{\sigma} \equiv m_2^{1/2} = \sqrt{\frac{1}{n}\sum_{i=1}^{n}(x_i - \hat{\mu})^2} \equiv \sqrt{\frac{1}{650}\sum_{i=1}^{650}[(F_{YI})_i - \hat{\mu}]^2}$	Provides a measure of the data spread around the sample mean
Skewness	$\hat{\gamma}_1 \equiv \frac{m_3}{\hat{\sigma}^3} = \left[\frac{1}{n}\sum_{i=1}^{n}(x_i - \hat{\mu})^3\right] / \sqrt{\left[\frac{1}{n}\sum_{i=1}^{n}(x_i - \hat{\mu})^2\right]^3}$	Asymmetry of the data around the median.; a negative skew (left) has fewer large values and a positive skew (right) has fewer low values.
Kurtosis	$\hat{k} \equiv \frac{m_4}{\hat{\sigma}^4} = \left[\frac{1}{n}\sum_{i=1}^{n}(x_i - \hat{\mu})^4\right] / \sqrt{\left[\frac{1}{n}\sum_{i=1}^{n}(x_i - \hat{\mu})^2\right]^4} - 3$	A high kurtosis value indicates that the distribution has a sharp peak with long and fat tails.
COV	$= \hat{\sigma}/\mu$	Coefficient of variation, indicating the dispersion of the distribution, normalized to the mean

Table A.2 Fitting curves.

Distribution Name			Distribution fitting function	Notes
Birnbaum-Saunders	$a = \sqrt{(x_i - \alpha)/\beta}$ $z = (a^2 - 1)/a\gamma$ $\varphi = Nor.Stand.Distr.$	:	$[(a^2 + 1)/2a\gamma(x_i - \alpha)] \cdot \varphi(z)$	Fitting parameters: α = location β = scale γ = shape
Gamma	$\Gamma(c) = \int_0^\infty t^{c-1}e^{-t}\,dt$ Gamma function (Integral form)	:	$\{1/[b \cdot \Gamma(c)]\}(x_i/b)^{(c-1)}exp\,(-x_i/b)$	Fitting parameters: c = shape b = scale
Inverse gaussian	$z_i = ln\,(x_i/\theta)$ $\varphi = Nor.Stand.Distr.$	:	$\{\sqrt{\beta}/[x_i \cdot exp\,(z_i/2)]\} \cdot \varphi(z_i)$	Fitting parameters: θ = mean β = scale
Laplace		:	$(\lambda/2) \cdot exp[-\lambda\lvert x - \mu\rvert]$	Fitting parameters: μ = mean λ = scale
Largest and Smallest Extreme Value	$z_i = (x_i - \alpha)/\beta$	:	$\{exp[-z_i - \exp\,(z_i)]\}/\beta$	Fitting parameters: α = location β = scale
Logistic	$z_i = (x_i - \mu)/\sigma$	:	$exp(z_i)\,/\{(1/\sigma) \cdot [1 + exp\,(z_i)]^2\}$	Fitting parameters: μ = mean σ = standard deviation
Loglogistic	$z_i = (lnx_i - \mu)/\sigma$	:	$exp(z_i)\,/\{[1/(\sigma \cdot x_i)] \cdot [1 + exp\,(z_i)]^2\}$	Fitting parameters: $exp\,(\mu)$ = median σ = scale
Lognormal		:	$\left[1/(\sqrt{2\pi} \cdot \sigma \cdot x_i)\right]exp\,[-(lnx_i - \mu)^2/(2\sigma^2)]$	Fitting parameters: μ = mean σ^2 = variance
Normal		:	$\left[1/(\sqrt{2\pi} \cdot \sigma)\right]exp\,[-(x_i - \mu)^2/(2\sigma^2)]$	Fitting parameters: μ = mean σ^2 = variance
Weibull		:	$(\alpha/\beta^\alpha) \cdot x_i^{(\alpha-1)} \cdot exp\,[-(x_i/\beta)^\alpha]$	Fitting parameters: α = shape β = scale

Table A.3 Results of the numerical experiments.

mesh numb	depth (m)	level	$\mu_{\Delta R1}$	$\mu_{\Delta R2}$	$\mu_{\Delta R3}$	$\mu_{\Delta R4}$	$\sigma_{\Delta R1}$	$\sigma_{\Delta R2}$	$\sigma_{\Delta R3}$	$\sigma_{\Delta R4}$
1	0.11	superf	1.2468	**1.2424**	1.2461	1.2457	0.03398	**0.02846**	0.02827	0.02508
2	1.35	superf	1.0258	**1.0243**	1.0253	1.0247	0.0137	**0.0122**	0.0123	0.0124
3	2.12	superf	1.1324	**1.1276**	1.1313	1.1307	0.0357	**0.0296**	0.0305	0.0270
4	2.17	superf	1.0111	**1.0109**	1.0111	1.0111	0.0018	**0.00152**	0.00153	0.00137
5	2.62	superf	1.2027	**1.2006**	1.2026	1.2027	0.0199	**0.0180**	0.01754	0.0160
6	2.69	superf	2.0224	**2.0118**	2.0197	2.0191	0.0812	**0.0672**	0.0682	0.0611
7	3.85	superf	1.4337	**1.4276**	1.4332	1.4334	0.0548	**0.0489**	0.0475	0.0431
8	4.16	interm	2.8327	**2.8193**	2.8308	2.8299	0.1086	**0.0941**	0.0949	0.08455
9	4.20	interm	1.7118	**1.7063**	1.7110	1.7112	0.04512	**0.0386**	0.03722	0.03356
10	4.69	interm	1.7729	**1.7661**	1.7726	1.7722	0.0597	**0.0531**	0.0514	0.0470
11	6.33	interm	1.3319	**1.3278**	1.3316	1.3317	0.0356	**0.0313**	0.0302	0.0271
12	6.43	interm.	1.0087	**1.0071**	1.0079	1.0073	0.0087	**0.0052**	0.0066	0.0053
13	6.66	interm	3.2376	**3.2236**	3.2357	3.2355	0.1104	**0.0932**	0.0896	0.0794
14	6.81	interm	2.7697	**2.7606**	2.7686	2.7684	0.07665	**0.06657**	0.06485	0.05878
15	11.90	deep	2.5239	**2.5184**	2.5234	2.5233	0.04412	**0.03810**	0.03727	0.03262
16	12.13	deep	2.5051	**2.4976**	2.5037	2.5035	0.0546	**0.04247**	0.04049	0.03467
17	12.98	deep	2.1194	**2.1147**	2.1192	2.1189	0.03726	**0.03185**	0.03053	0.0268
18	13.07	deep	2.4951	**2.4900**	2.4958	2.4957	0.04604	**0.04137**	0.03781	0.03324
19	16.37	deep	1.7468	**1.7436**	1.7472	1.7475	0.02871	**0.02479**	0.02099	0.01806
20	16.82	deep	1.3894	**1.3873**	1.3893	1.3893	0.0171	**0.01483**	0.01375	0.01229
21	17.38	deep	2.5366	**2.5318**	2.5362	2.5364	0.03634	**0.02785**	0.02353	0.0192
22	18.63	deep	2.6866	**2.6829**	2.6871	2.6877	0.0326	**0.02784**	0.02232	0.01813
23	21.66	deep	2.3324	**2.3300**	2.3321	2.3320	0.01932	**0.0151**	0.0142	0.01249
24	31.31	deep	2.4598	**2.4567**	2.4598	2.4612	0.02612	**0.0228**	0.02131	0.01994
25	35.54	deep	2.2037	**2.1998**	2.2035	2.2039	0.03696	**0.0288**	0.02635	0.02296

Table A.4a Goodness of fit by the MLLT.

Node numb	Depth (m)	Birnbaum-Saunders		Gamma		Inverse Gaussian		Laplace		Larg. Extr. (L)	Smal. Val. (S)
		Cohes.	F_{YI}	Cohes.	F_{YI}	Cohes.	F_{YI}	Cohes.	F_{YI}	Cohes.	F_{YI}
1	0.11	**12115**	1280	10372	1279	11948	1280	3722	1267	5196 L	1254 L
2	1.35	no fit	1872	**3729**	1870	no fit	1872	2787	2032	3657 L	**2050 L**
3	2.12	no fit	1251	1891	1249	no fit	1251	1643	1232	**2136 L**	**1262 L**
4	2.17	-1548	3181	1847	3181	-2440	3181	1649	**3196**	**2085 L**	3184 L
5	2.62	-2940	**1623**	833	**1623**	no fit	**1623**	934	1592	1189 L	1582 L
6	2.69	no fit	718	796	716	no fit	718	863	715	1145 L	720 L
7	3.85	-4062	**965**	-358	**965**	no fit	**965**	172	940	-3 L	923 L
8	4.16	no fit	**523**	-257	522	no fit	**523**	356	511	10 L	501 L
9	4.20	-3827	1093	-409	1093	no fit	1093	189	1099	-143 L	1048 L
10	4.69	-2960	910	-313	910	no fit	910	223	877	-241 L	865 L
11	6.33	-1456	1245	370	**1245**	no fit	**1245**	1261	1219	-159 L	1189 L
12	6.43	-391	2168	720	2164	no fit	2167	1364	2472	117 L	**2489 L**
13	6.66	-9971	512	781	511	no fit	512	1588	526	153 L	459 L
14	6.81	-486	749	1022	748	no fit	749	1701	721	303 L	709 L
15	11.90	5807	1107	5897	1107	5807	1107	**7063**	1108	no fit	1061 L
16	12.13	6362	975	6448	973	6362	975	**7656**	**1039**	no fit	944 L
17	12.98	7119	1217	7180	1217	7119	1217	**8561**	**1242**	no fit	1154 L
18	13.07	7273	1075	7322	1077	7273	1075	**8673**	**1111**	no fit	1042 S
19	16.37	10455	1384	10516	1384	10455	1384	**12397**	**1476**	no fit	1249 L
20	16.82	10969	1723	10998	1723	10969	1723	**12816**	1729	8717 S	1644 L
21	17.38	11110	1236	11135	1235	11110	1236	**12965**	**1384**	no fit	1142 L
22	18.63	11322	1302	11340	1303	11322	1302	**13089**	**1449**	8777 S	1120 S
23	21.66	8683	1648	8704	1646	8683	1648	**10377**	**1712**	no fit	1617 L
24	31.31	280	1446	314	1446	280	1446	285	**1467**	320 **S**	1380 S
25	35.54	2091	1236	2226	1231	2091	1236	3803	**1327**	**5250 S**	1193 L

Table A.4b Goodness of fit by the MLLT.

Node numb	Depth (m)	Logistic		Loglogistic		Lognormal		Normal		Weibull	
		Cohes.	F_{YI}	Cohes.	F_{YI}	Cohes.	F_{YI}	Cohes.	F_{YI}	Cohes.	F_{YI}
1	0.11	3056	1286	10885	**1288**	11400	1280	2347	1276	10613	1176
2	1.35	2408	1882	3493	1888	2618	1872	1912	1866	3716	1528
3	2.12	1525	1250	1452	1253	438	1251	1270	1244	2091	1142
4	2.17	1519	3187	1381	3187	467	3181	1265	3180	2060	2815
5	2.62	968	1614	322	1614	-722	1623	856	1622	**1217**	1514
6	2.69	886	724	321	**728**	-773	718	751	710	**1150**	585
7	3.85	**303**	960	-585	960	-1844	965	230	965	194	913
8	4.16	**459**	518	-377	520	-1712	**523**	376	521	293	455
9	4.20	**323**	**1102**	-543	**1102**	-1800	1093	243	1092	153	997
10	4.69	**367**	904	-329	905	-1439	**910**	272	909	164	851
11	6.33	**1288**	1243	686	1243	-511	1245	1088	**1245**	884	1192
12	6.43	**1403**	2308	955	2314	93	2167	1214	2159	1004	no fit
13	6.66	**1590**	526	1135	**527**	no fit	512	1334	510	1038	417
14	6.81	**1727**	748	1343	749	372	**749**	1514	747	1242	666
15	11.90	6589	**1113**	6523	**1113**	5820	1107	5975	1106	4845	921
16	12.13	7184	1018	7109	1020	6374	975	6530	968	no fit	no fit
17	12.98	7954	1233	7905	1234	7127	1217	7235	1216	5900	993
18	13.07	8109	1097	8073	1097	7282	1076	7351	1079	5594	1006
19	16.37	11638	1441	11609	1439	10464	1384	10584	1386	no fit	662
20	16.82	12025	**1737**	12006	**1737**	10972	1723	11029	1723	9196	1497
21	17.38	12177	1331	12164	1331	11114	1236	11159	1232	no fit	no fit
22	18.63	12337	1392	12325	1390	11325	1302	11356	1304	9278	no fit
23	21.66	9643	1707	9628	1708	8686	1648	8723	1643	no fit	no fit
24	31.31	**433**	1465	398	1465	282	1446	360	1447	-96	1284
25	35.54	3188	1316	2937	1316	2937	1236	2480	1221	5040	no fit